







# Quantum Chemical Modeling, Synthesis, Spectroscopic (FT-IR, Excited States, UV/VIS) Studies, FMO, QTAIM, ELF, LOL, NBO, NLO and QSAR Analyses of Nelarabine

Evgeniy Kvasnyuk <sup>1</sup>, Aliaksei Sysa <sup>1</sup>, Sultan Al Saud <sup>1,4,\*</sup>, Siyamak Shahab <sup>1,3,4</sup>, Masoome Sheikhhi <sup>5</sup>, Sadegh Kaviani <sup>6</sup>, Anatoliy Zinchenko <sup>2</sup>

<sup>1</sup> International Sakharov Environmental Institute, Belarusian State University, 23 Dolgobrodskaya street, Minsk 220009, Republic of Belarus

<sup>2</sup> Institute of Microbiology of the National Academy of Sciences of Belarus, 5/2 Academic V.F. Kuprevich street, Minsk 220141, Republic of Belarus

<sup>3</sup> Institute of Physical Organic Chemistry, National Academy of Sciences of Belarus, 13 Surganov Str., Minsk 220072

<sup>4</sup> Institute of Chemistry of New Materials, National Academy of Sciences of Belarus, 36 Skarina Str., Minsk 220141

<sup>5</sup> Young Researchers and Elite Club, Gorgan Branch, Islamic Azad University, Gorgan, Iran

<sup>6</sup> Mashhad, Iran, Ferdowsi University of Mashhad

\* Correspondence: [sultan@compchemresearch.com](mailto:sultan@compchemresearch.com) (S.A.);

Scopus Author ID: 57219870719

Received: 30.12.2021; Accepted: 29.01.2022; Published: 27.03.2022

**Abstract:** In this study, we report the results of experiments and density functional theory (DFT), time-dependent DFT, and quantitative structure-activity relationship (QSAR) analyses of (2R,3S,4S,5R)-2-(2-amino-6-methoxy-9H-purin-9-yl)-5-(hydroxymethyl) tetrahydrofuran-3,4-diol (nelarabine). The molecular geometry, vibrational modes, excited states, molecular electrostatic potential (MEP) maps were calculated and discussed. Frontier molecular orbitals (FMO), quantum theory of atoms in molecules (QTAIM), electron localization function (ELF), localized orbital locator (LOL), natural charge, natural bonding, orbital (NBO) analysis were conducted and discussed. Nonlinear optical (NLO) and thermodynamic parameters were determined and discussed. In addition, Fourier transform infrared (FT-IR) and ultraviolet/visible (UV-Vis) spectral parameters were calculated and were found to agree with experimental spectral parameters excellently. The physicochemical, pharmacokinetic, and pharmacodynamic profiles were determined. The applicability of nelarabine as an anticancer drug was investigated in terms of QSAR models, and positive conclusions were yielded.

**Keywords:** nelarabine; NBO; ELF; QTAIM; QSAR; DFT.

© 2022 by the authors. This article is an open-access article distributed under the terms and conditions of the Creative Commons Attribution (CC BY) license (<https://creativecommons.org/licenses/by/4.0/>).

## 1. Introduction

Nucleosides are a group of naturally occurring molecules subunits of RNA and DNA. They are composed of nucleobase, purine or pyrimidine, and a five-carbon sugar. The purine bases include guanine and adenine, and the pyrimidine bases are uracil, thymine, and cytosine. The five-carbon sugar is deoxyribose or ribose in DNA or RNA, respectively. Nucleosides and their analogs have been long applied in medical and biochemical fields. Several nucleoside analogs have been clinically approved to treat different types of cancers, bacterial and fungal infections, and viral and parasitic diseases. Many other nucleosides are currently undergoing preclinical and clinical trials [1].

Along with fludarabine and cladribine, Nelarabine represents a new generation of compounds with anticancer and antiviral activities [2-4]. The first study regarding nelarabine was published in 1981 [5]; in 2005 and 2007, nelarabine was registered in the USA and Europe to treat acute lymphoblastic leucosis. Because nelarabine exhibits high potency and activity, several chemical and biochemical methods have been developed for its synthesis (Scheme S1-S6) (Supplementary Material). Nelarabine is a purine antimetabolite and an analog of deoxyguanosine. Nelarabine is a prodrug; its derivative—arabinofuranosylguanine (ara-GTP) obtained after transformation to a 5'-triphosphate derivative—can inhibit DNA synthesis with cytostatic effects. Nelarabine exhibits approximately 10-fold higher solubility in water, making it more advantageous as an anticancer substance compared to ara-GTP [3,4]. However, the complicated synthesis of nelarabine limits its application. In addition, the structural and biological properties of nelarabine are not completely understood. Thus, further investigation of nelarabine is required.

This manuscript reports the results of experiments, DFT, TD-DFT, and QSAR analyses of nelarabine to investigate further its stability, reactivity, structural properties, and pharmacological properties.

## 2. Materials and Methods

### 2.1. Experimental methods.

The progress of all reactions and purity of the synthesized compounds were monitored by thin-layer chromatography (TLC) on Kieselgel 60 F<sub>254</sub> plates. Column chromatography was performed with silica gel (200–400 mesh). High-resolution mass spectra were recorded in the ESI mode with a Waters 2998 mass spectrometer. The UV-Vis spectrum of nelarabine was recorded in a 9:1 mixture of phosphate buffer (pH 7.0) and ethanol with a Shimadzu UV-1650 PC UV-visible spectrophotometer. The FT-IR spectrum was measured using an IR Affinity-1 infrared spectrometer with the KBr pellet method. The purity of nelarabine (99.73%) was determined through HPLC by using a Shimadzu liquid chromatograph with a Zorbax Eclips column (C-18, 25 × 4.6 mm); a mixture of acetonitrile and aqueous NH<sub>4</sub>H<sub>2</sub>PO<sub>4</sub> (pH 7.0) was used as the eluent.

#### 2.1.1. 9-(2',3',5'-Tri-O-acetyl-β-D-arabinofuranosyl)guanine (20).

Triethylamine (29 g, 40 mL, 0.29 mol) was added in portions to a magnetically stirred suspension of 9-(β-D-arabinofuranosyl)guanine (19) (25 g, 88.25 mmol), 4-*N,N*-dimethylaminopyridine (0.75 g, 6.15 mmol), and acetic anhydride (38 g, 60 mL, 0.37 mol) in acetonitrile (150 mL). The mixture was stirred magnetically for 30 min and filtered; the filtrate was evaporated *in vacuo*. Ethanol (100 mL) was added to the residue, which was then evaporated. An additional portion of ethanol (100 mL) was added to the residue and cooled in a refrigerator. A white precipitate was collected by filtration and washed with cooled ethanol (3 × 30 mL). The crystalline product was air-dried and then dried *in vacuo* at 90 °C to obtain 20 (32.5 g). TLC confirmed the purity of 20. Compound 20 was used as received without further purification in the next step.

#### 2.1.2. 2-Amino-6-chloro-9-(2',3',5'-tri-O-acetyl- $\beta$ -D-arabinofuranosyl)purine (21).

Phosphorous oxychloride (37.5 mL, 61.7 g, 0.4 mol) was added to a mixture of 20 (32.5 g, 79.25 mmol), benzyl triethylammonium chloride (36.5 g, 158 mmol), *N,N*-dimethylaniline (10.1 mL, 9.7 g, 80 mmol), and acetonitrile (150 mL) in a 1 L flask fitted with a magnetic stirrer and a reflux condenser. The flask was placed in an oil bath preheated to 110 °C. The mixture was heated to reflux, and heating continued for another 10 minutes. Then, the mixture was concentrated in vacuo, and the residue was treated with chloroform (250 mL). The solution was added to crushed ice (150 g), and the mixture was stirred for 20 min. The layers were separated, and the aqueous layer was extracted with chloroform (3  $\times$  50 mL). The combined organic extracts were washed with water (3  $\times$  50 mL) and then with portions of saturated sodium bicarbonate until the mixture's pH was neutral. The final solution was washed with water (3  $\times$  50 mL), dried over Na<sub>2</sub>SO<sub>4</sub>, and filtered. The solution was treated with active carbon (2 g), filtered, and evaporated in vacuo to obtain 21 (31.25 g) in a powder form.

#### 2.1.3. 2-Amino-6-chloro-9-( $\beta$ -D-arabinofuranosyl)purine (22).

A solution of potassium carbonate (1.1 g) in methanol (110 mL) was added to a solution of 21 (31.25 g, 73 mmol) in methanol (150 mL). The resulting solution was stirred at 50–60 °C for 1.5 h. The solution was added to an ion exchange resin Dowex50Wx8 (H<sup>+</sup>-form, 200 mesh) in order to neutralize the reaction. The ion exchange resin was filtered out, and the solution was washed with methanol (3  $\times$  5 mL) and water (3  $\times$  5 mL). Active carbon (1 g) was added to the combined methanol and water solution, and the mixture was heated with stirring at 40–50 °C. Then, the mixture was cooled to room temperature, and the active carbon was filtered and washed with methanol (3  $\times$  10 mL). The combined solutions were evaporated to dryness in vacuo. The residue was treated with ethanol (25 mL), and the mixture was kept at room temperature for 16 h. The obtained solid was collected, washed with cooled ethanol (2  $\times$  10 mL), and dried at room temperature initially and then at 90 °C for 5 h to obtain a chloro derivative (22; 15.5 g) as a yellow powder.

#### 2.1.4. Nelarabine.

Compound 22 (15.5 g, 51.25 mmol) was added with stirring to a solution of sodium methylate (15 g, 278 mmol) in methanol (250 mL). The solution was stirred at room temperature for 2–3 h until no starting material was observed via TLC. The resulting solution was acidified to attain a pH of 6–7 by using concentrated HCl, and the precipitated NaCl was filtered and washed with methanol (2  $\times$  10 mL). Silica gel (15 g) was added to the combined methanol solution, and the resulting mixture was evaporated in vacuo to dryness. The residue was added to the top of the prepacked column for chromatography with silica gel (60 g). The column was eluted with a mixture of chloroform and methanol (9:1). Fractions containing nelarabine were collected and evaporated in vacuo for crystallization. The precipitate was filtered, washed with cooled chloroform (2  $\times$  10 mL), dried, and recrystallized using hot water to obtain a solid that was dried in vacuo at 70 °C to yield nelarabine (11.5 g) as white crystals. The total yield of nelarabine was 43.8%. Literature mp 208–210 °C [6], observed mp 211–212 °C. HRMS calculated for C<sub>11</sub>H<sub>16</sub>N<sub>5</sub>O<sub>5</sub> [M+H]<sup>+</sup> 298.2752, found 298.2752. The purity of nelarabine was 99.73%, as determined by HPLC analysis.

## 2.2. Computational methods.

Quantum chemical calculations were performed on nelarabine via the density functional theory (DFT) and time-dependent density functional theory (TD-DFT) by using Gaussian 09 W [7], Multiwfn [8], NBO 6.0 [9], and the Gaussview molecular visualization program. Pharmacological investigations were performed using the online software Pre-ADMET [10], SwissADME [11], PASSOnline [12], CLC-Pred [13], SOMP [14], and MetaTox [15] based on quantitative structure-activity relationship models. Conformational analysis was conducted to locate the conformation with the lowest energy, subsequently used as the input for geometry optimization. Calculations of the IR and UV-Vis spectra in addition to frontier molecular orbitals (FMOs), quantum theory of atoms in molecules (QTAIMs), natural bond orbitals (NBOs), nonlinear optics (NLOs), and thermodynamic properties were conducted using Becke's three-parameter hybrid density functional (B3LYP) with a 6-31G\* basis set. The conductor-like polarizable continuum model (CPCM) utilizing universal force-field radii was used for the UV-Vis calculations in ethanol; the simulated results were compared with the experimental results. All other calculations were computed in the gas phase.

## 3. Results and Discussion

### 3.1. Optimized structure of nelarabine.

The optimized geometry of the lowest energy conformation of nelarabine is illustrated in Figure 1, with selected calculated bond lengths and angles listed in Table 1. The conformation with the lowest energy exhibits higher stability through hydrogen bonding relative to other low-energy conformations. The purine moiety exhibits shorter bonds and wider angles between bonds relative to the sugar moiety, implying greater charge delocalization and conjugation within the purine moiety relative to the sugar moiety.

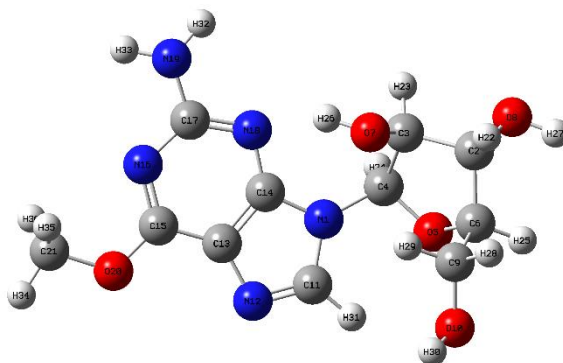


**Figure 1.** Optimized molecular structure of Nelarabine.

**Table 1.** Ground state geometric parameters of selected bonds in Nelarabine.

Parameter	Bond Length (Å)	Parameter	Bond Angle (°)
N1-C4	1.475	N1-C4-O5	108.76
N1-C11	1.393	N1-C11-N12	113.89
N1-C14	1.373	N1-C14-N18	127.59
C2-O8	1.423	C2-C3-O7	108.75
C3-O7	1.407	C2-C6-O5	103.72
C4-O5	1.407	C3-C2-O8	106.48
O5-C6	1.437	C4-C3-C7	114.88
O7-H26	0.981	C4-C5-C6	109.74
O8-H27	0.976	C6-C2-C8	111.97
C9-O10	1.422	C6-C9-O10	107.62
O10-H30	0.969	C11-N1-N14	105.58
C11-N12	1.309	C11-N12-C13	104.04

Parameter	Bond Length (Å)	Parameter	Bond Angle (°)
N12-C13	1.385	N12-C13-C14	110.93
C14-N18	1.345	C13-C14-N18	126.81
C15-N16	1.33	C13-C15-N16	120.64
C15-O20	1.336	C14-N18-C17	112.21
N16-C17	1.353	C15-O20-C21	117.52
C17-N18	1.343	N16-C15-O20	120.16
C17-N19	1.373	N16-C17-N19	115.77
N19-H32	1.01	N18-C17-N16	127.13
N19-H33	1.01	N18-C17-N19	117.07
O20-C21	1.433	H32-N19-H33	116.53

### 3.2. Vibrational analysis.

Nelarabine consists of 36 atoms, which exhibit 102 normal modes of IR active vibrations. In the spectrum, peaks were observed in the 1000–1650 cm<sup>-1</sup> range, attributed to C-N stretching, C=N stretching, C=C stretching, C-O stretching, N-H bending, O-H bending, and C-H bending. Moreover, the 2900–3500 cm<sup>-1</sup> peaks are ascribed to O-H stretching, N-H stretching, and C-H stretching. Minor peaks are apparent in the 500–900 cm<sup>-1</sup> fingerprint region, attributed to double and single bond bending and torsional vibrations. The theoretical IR spectrum is in excellent agreement with the experimental FT-IR spectrum (Table 2).

**Table 2.** Experimental and theoretical vibrational frequencies of Nelarabine and their peak assignments

vexp(cm <sup>-1</sup> )	vcal(cm <sup>-1</sup> )	IR intensity	Assignments
3789.98w	3762.89	20.9233	vO-H
	3747.41	17.8099	vO-H
	3711.84	32.6844	vN-H asym
3483.72s	3593.5	58.0916	vN-H sym
3378.09s	3543.96	432.1319	vO-H
3240m	3302.89	6.79	vC-H(purine)
	3177.25	22.0944	vC-H(OCH3) asym
3149.46m	3143.61	23.9706	vC-H(OCH3) asym
	3087.74	65.3046	vC-H(sugar), vC-H(CH2) asym
	3080.79	48.19	vC-H(sugar), vC-H(CH2) asym
	3070.47	50.5955	vC-H(OCH3) sym
	3068.43	7.1591	vC-H(sugar), vC-H(CH2) asym
	3064.53	8.0966	vC-H(sugar), vC-H(CH2) asym
	3053.59	37.7953	vC-H(sugar), vC-H(CH2) asym
2919.46m	2987.42	57.339	vC-H(CH2) sym
1625.84s	1666.47	446.2543	sN-H, vC=C asym, vC=N asym
	1648.22	204.2503	sN-H, vC=C asym, vC=N asym
1590.96s	1625.6	463.7515	sN-H, vC=C asym, vC=N asym, vC-O (purine), sC-H(OCH3)
	1553.72	39.1589	sN-H, vC=C asym, vC=N asym, vC-O (purine), sC-H(OCH3)
	1548.02	3.9153	sC-H(CH2)
	1531.25	91.8704	rN-H, vC=C asym, vC=N asym, vC-O(purine), sC-H(OCH3)
	1524.04	33.9569	sC-H(OCH3), vC=N sym
1517.02w	1511.18	5.4749	twC-H(OCH3)
1486.23m	1499.1	97.08	sN-H, vC=N sym, sC-H(OCH3), sO-H
	1483.85	2.3575	wC-H(CH2), sO-H, wC-H(sugar)
	1480.81	13.6795	wC-H(CH2), sO-H, wC-H(sugar), vC-C(sugar) sym
1450.19m	1456.09	119.9852	rN-H, vC=C sym, vC=N asym, sC-H(OCH3), wC-H(sugar)
	1448.16	157.995	sC-H(OCH3), vC-O(purine)
1412.03w	1417.69	19.0834	wC-H(sugar), wC-C(sugar) sym, sO-H
	1409.46	18.1786	wC-H(sugar), wC-C(sugar) sym, sO-H
1396.39m	1386.65	56.0495	rN-H, vC=C asym, vC=N asym, wC-H(sugar), wC-H(purine), sO-H
1383.49m	1382.03	42.4661	rN-H, vC=C asym, vC=N asym, wC-H(sugar), wC-H(purine), sO-H
	1379.05	31.3027	wC-H(sugar), wC-C(sugar) sym, sO-H, wC-H(purine)
	1362.24	38.4271	wC-H(sugar), wC-C(sugar) sym, sO-H, wC-H(purine)
	1353.47	0.852	vC-N(purine), wC-H(sugar), wC-C(sugar) sym, sO-H, wC-H(purine)
1330.68w	1342.77	20.0625	vC-N(purine), wC-H(sugar), wC-C(sugar) sym, sO-H, wC-H(purine), vC=C asym
1310.14w	1319.96	27.234	wC-H(sugar), wC-C(sugar) sym, sO-H
			vC-N(purine), wC-H(sugar), vC-O(purine), twC-H(CH2), wC-H(OCH3), vC-O(sugar) asym
1264.49s	1289.2	210.733	
1254.56s	1280.69	126.3047	vC-N(purine), wC-H(sugar), vC-O(purine), twC-H(CH2), wC-H(OCH3)



vexp(cm <sup>-1</sup> )	vcal(cm <sup>-1</sup> )	IR intensity	Assignments
	1264.59	33.7886	wC-H(sugar), wC-C(sugar) sym, sO-H
	1246.01	21.589	wC-H(sugar), wC-C(sugar) sym, sO-H, vC-N(purine), vC-O(purine)
	1237.81	62.836	wC-H(sugar), wC-C(sugar) sym, sO-H, vC-N(purine), sC-H(purine), vC=C sym
1212.17m	1228.18	43.3561	wC-H(sugar), wC-C(sugar) sym, sO-H, vC-N(purine), sC-H(purine)
	1224.64	32.7808	wC-H(sugar), wC-C(sugar) sym, sO-H, vC-N(purine), sC-H(purine)
	1218.96	9.2555	vC=N sym, twC-H(OCH3), sC-H(purine)
	1182.06	0.6382	twC-H(OCH3)
1143.24m	1143.88	137.04	vC-O(sugar) asym, wC-H(sugar)
	1129.81	59.025	vC-O(sugar) asym, wC-H(sugar)
	1119.37	20.2806	twN-H(purine), vC=N asym, twC-H(OCH3)
1122.19m	1112.98	65.1524	vC-O(sugar) asym
	1103.58	4.2146	vC-O(sugar) asym, vC-O(purine), vC-N(purine), sO-H, vC=N sym
1055.67s	1096.99	193.9747	vC-O(sugar), vC-O(purine), vC-N(purine), sO-H, vC=N sym, rC-H(sugar), VC=C sym
	1062.76	49.9339	vC-O(sugar), vC-O(purine), vC-N(purine), sO-H, vC=N sym, rC-H(sugar)
	1049.56	13.7818	vC-O(sugar), vC-O(purine), vC-N(purine), vC=N sym, rC-H(sugar)
	1036.5	38.5077	vC-O(sugar) sym
1021.91m	1018.57	51.616	vC-O(sugar) sym, vC-O(purine), rC-H(sugar), sC=N
	992.78	13.7158	rC-O(sugar), sC=N, vC-O(purine), toC-H(sugar)
967.37w	967.72	32.762	rC-O(sugar), sC=N, vC-O(purine), toC-H(sugar), vC-C(sugar)
899.92w	913.52	11.2576	rC-O(sugar), sC=N, toC-H(sugar), vC-C(sugar), toO-H
877.61w	878.35	26.6366	rC-O(sugar), toC-H(sugar), vC-C(sugar), toO-H, toC-H(CH2)
	861.64	7.2134	toC-H(sugar), sC-H(purine)
	851.21	5.459	toC-H(sugar), sC-H(purine), sC=N, vC-C(sugar)
807.5w	843.7	7.8561	toC-H(sugar), toO-H, sC=N, toC-H(CH2)
	791.32	21.8785	sC-C(sugar), toC-H(sugar), wC=N, wC=C, toO-H, toC-H(CH2)
	789.98	7.7348	sC-C(sugar), toC-H(sugar), wC=N, wC=C, toO-H, toN-H, toC-H(CH2)
790.33m	748.6	135.2178	sC-C(sugar), toC-H(sugar), wC=N, wC=C, toO-H, toN-H, toC-H(CH2)
	740.48	0.6338	toC-C(sugar), toC-H(sugar), wC=N, wC=C, toO-H, toN-H, to C-H(OCH3), toC-H(CH2)
	729.03	66.3556	toC-C(sugar), toC-H(sugar), wC=N, wC=C, toO-H, toN-H, to C-H(OCH3), toC-H(CH2)
696.29w	699.26	31.7664	toC-C(sugar), toC-H(sugar), wC=N, wC=C, toO-H, toN-H, to C-H(OCH3), to C-O(sugar), toC-H(CH2)
	677.55	21.4734	toC-C(sugar), toC-H(sugar), wC=N, wC=C, toO-H, toN-H, to C-H(OCH3), to C-O(sugar), toC-H(CH2)
663.17w	664.03	8.705	toC-C(sugar), toC-H(sugar), sC=N, sC=C, toO-H, to C-H(OCH3), to C-O(sugar), toC-H(CH2)
644.81w	642.65	30.4178	toC-C(sugar), toC-H(sugar), sC=N, sC=C, toO-H, to C-H(OCH3), to C-O(sugar), toC-H(purine), toC-H(CH2)
602.85w	592.95	8.5757	toC-C(sugar), toC-H(sugar), sC=N, sC=C, toO-H, to C-H(OCH3), to C-O(sugar), toC-H(purine), toC-H(CH2)
	581.92	15.7622	toC-C(sugar), toC-H(sugar), sC=N, sC=C, toO-H, to C-O(sugar), toC-H(purine), toC-H(CH2)
524.13w	515.85	10.2307	toC-C(sugar), toC-H(sugar), sC=N, sC=C, toO-H, to C-H(OCH3), to C-O(sugar), toC-H(CH2)
	501.55	31.7614	toC-C(sugar), toC-H(sugar), sC=N, sC=C, toO-H, to C-H(OCH3), to C-O(sugar), toC-H(purine), toC-H(CH2)

v, stretching; r, rocking; tw, twisting; w, wagging; to, torsion; sym, symmetric; asym, asymmetric, w, weak; m, medium; s, strong

### 3.3. MEP maps.

Molecular electrostatic potential (MEP) maps reflect regions with high or low electrostatic potential related to electron density and can be utilized to identify sites susceptible to electrophilic or nucleophilic attack and hydrogen bonding interactions [16-18]. The total electron density mapped with the electrostatic surface is illustrated in Figure 2. The negative sites with high electron density (prone to the electrophilic attack) are displayed in red, orange, and yellow. In contrast, the positive sites (which are prone to nucleophilic attack) are displayed in blue and cyan. The neutral regions are displayed in green. According to the MEP maps, the nitrogen and oxygen atoms in the modified purine moiety and the oxygen atoms in the sugar moiety are prone to electrophilic attack. The region between N12 and O20 on the modified

purine moiety and the oxygen atoms in the sugar moiety exhibit the highest susceptibility to electrophilic attack. In contrast, the hydrogen atoms bonded to the nitrogen atom in the modified purine moiety. The hydrogen atoms bonded to the oxygen atoms on the sugar moiety exhibit the highest susceptibility to nucleophilic attack. All other regions are relatively neutral.

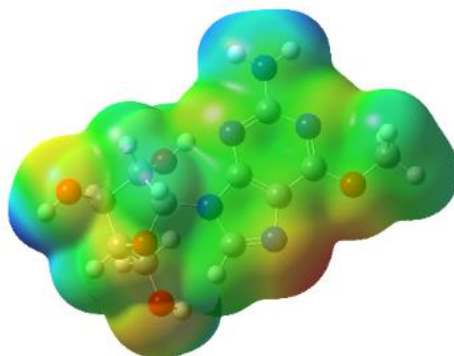


**Figure 2.** Total electron density mapped with the electrostatic surface of Nelarabine.

### 3.4. Electronic structure and excited states.

Twenty excited states of Nelarabine were calculated in ethanol and are listed in Table 3 [19,20]. The optimal transition was observed at  $\lambda = 213.46$  nm, oscillator strength  $f = 0.404$ , which is attributed to a charge transfer (CT) of one electron into the excited singlet state ( $S_0 \rightarrow S_4$ ), and is described by a wave function corresponding to the superposition of three configurations for the one-electron excitation: H-2 $\rightarrow$ LUMO (21%), H-1 $\rightarrow$ LUMO (54%), and HOMO $\rightarrow$ L+1 (18%). A transition at  $\lambda = 269.26$  nm, oscillator strength  $f = 0.341$  ( $S_0 \rightarrow S_1$ ) is the second most optimal transition, described by a wavefunction corresponding to a configuration for the one-electron excitation: HOMO $\rightarrow$ LUMO. A transition at  $\lambda = 234.96$  nm, oscillator strength  $f = 0.121$  ( $S_0 \rightarrow S_2$ ) is the third most optimal transition, which is described by a wavefunction corresponding to the superposition of three configurations for the one-electron excitation: H-2 $\rightarrow$ LUMO (12%), H-1 $\rightarrow$ LUMO (38%), HOMO $\rightarrow$ L+1 (43%). The shapes of the molecular orbitals involved in the  $\lambda_{\max} = 213.46$ , 234.96, and 269.26 nm transitions are presented in Figure 3. The theoretical excitation spectrum is in excellent agreement with the experimental UV-Vis spectrum of nelarabine in a 9:1 mixture of phosphate buffer (pH 7.0) and ethanol (absorption maxima at  $\lambda_{\max} = (210.8, 247.8, \text{ and } 279.8 \text{ nm})$ ).

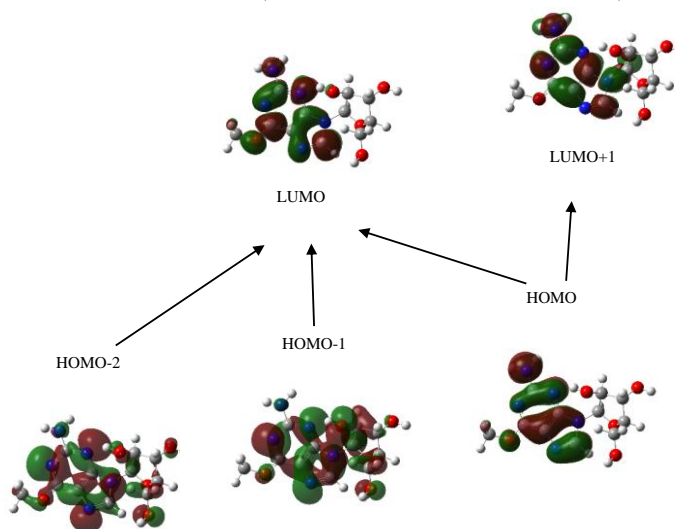


**Figure 3.** The shape of MOs involved forming the absorption spectrum of Nelarabine at  $\lambda_{\max} = (213.46, 234.96, \text{ and } 269.26 \text{ nm})$ .

**Table 3.** Calculated vertical excitation parameters of Nelarabine in ethanol.

Excited State	Energy (eV)	Wavelength (nm)	Configuration composition (corresponding transition orbitals)	Oscillator Strength (f)
S <sub>0</sub> →S <sub>1</sub>	4.60	269.26	HOMO→LUMO (95%)	0.341
S <sub>0</sub> →S <sub>2</sub>	5.28	234.96	H-2→LUMO (12%), H-1→LUMO (38%), HOMO→L+1 (43%)	0.121
S <sub>0</sub> →S <sub>3</sub>	5.28	234.67	H-2→LUMO (60%), HOMO→L+1 (32%)	0.080
S <sub>0</sub> →S <sub>4</sub>	5.81	213.46	H-2→LUMO (21%), H-1→LUMO (54%), HOMO→L+1 (18%)	0.404
S <sub>0</sub> →S <sub>5</sub>	5.98	207.40	H-8→LUMO (13%), H-7→LUMO (10%), H-3→LUMO (58%)	0.043
S <sub>0</sub> →S <sub>6</sub>	6.10	203.29	H-8→LUMO (19%), H-6→LUMO (14%), H-4→LUMO (22%), H-3→LUMO (28%)	0.026
S <sub>0</sub> →S <sub>7</sub>	6.12	202.51	H-2→L+1 (61%), H-1→L+1 (25%)	0.005
S <sub>0</sub> →S <sub>8</sub>	6.18	200.52	HOMO→L+2 (90%)	0.047
S <sub>0</sub> →S <sub>9</sub>	6.27	197.59	H-8→LUMO (18%), H-4→LUMO (66%)	0.075
S <sub>0</sub> →S <sub>10</sub>	6.37	194.51	H-5→LUMO (92%)	0.176
S <sub>0</sub> →S <sub>11</sub>	6.48	191.36	H-7→LUMO (48%), H-6→LUMO (43%)	0.124
S <sub>0</sub> →S <sub>12</sub>	6.65	186.38	H-2→L+1 (20%), H-1→L+1 (58%)	0.292
S <sub>0</sub> →S <sub>13</sub>	6.69	185.25	H-8→LUMO (36%), H-7→LUMO (33%), H-6→LUMO (22%)	0.014
S <sub>0</sub> →S <sub>14</sub>	6.82	181.83	H-3→L+1 (73%)	0.066
S <sub>0</sub> →S <sub>15</sub>	6.94	178.63	H-8→L+1 (18%), H-6→L+1 (12%), H-4→L+1 (26%), H-2→L+2 (13%)	0.002
S <sub>0</sub> →S <sub>16</sub>	7.03	176.31	H-9→LUMO (20%), H-5→L+1 (11%), H-4→L+1 (25%), H-2→L+2 (13%)	0.008
S <sub>0</sub> →S <sub>17</sub>	7.13	173.91	HOMO→L+3 (83%)	0.010
S <sub>0</sub> →S <sub>18</sub>	7.16	173.20	H-9→LUMO (18%), H-5→L+1 (13%), H-1→L+2 (17%)	0.092
S <sub>0</sub> →S <sub>19</sub>	7.20	172.12	H-8→L+1 (17%), H-6→L+1 (17%), H-4→L+1 (26%), H-2→L+2 (10%)	0.021
S <sub>0</sub> →S <sub>20</sub>	7.24	171.17	H-9→LUMO (29%), H-5→L+1 (56%)	0.007

### 3.5. Frontier molecular orbital analysis and electronic properties.

FMO analysis was performed to investigate nelarabine's electronic properties, optical properties, and chemical reactivity. The highest occupied molecular orbital (HOMO) and the lowest unoccupied molecular orbital (LUMO) are typically significant for electron donation and electron acceptance. The gas-phase electron density of the HOMO and LUMO are primarily localized on the modified purine moiety. The molecular orbitals in the gas phase and solution are relatively identical, except for energy gaps, which are smaller in ethanol ( $E_{\text{HOMO}} \uparrow$ ,  $E_{\text{LUMO}} \downarrow$ ). The path of the FMO electronic transitions (CT) in nelarabine is primarily within the modified purine moiety due to the presence of  $\pi$  bonds within the modified purine moiety.

The HOMO and LUMO energy levels ( $E_{\text{HOMO}}$  and  $E_{\text{LUMO}}$ ) are related to the ionization potential ( $I = -E_{\text{HOMO}}$ ) and electron affinity ( $A = -E_{\text{LUMO}}$ ), respectively. The global hardness ( $\eta$ ) is defined as the resistance of an atom or a group of atoms to CT. Electronegativity ( $\chi$ ) measures the power of an atom or a group of atoms to attract electrons. The electronic potential ( $\mu$ ) is a measure of the tendency of an electron in an atom or a group of atoms to escape its ground state. The chemical softness ( $S$ ) measures the capacity of an atom or a group of atoms to receive electrons. Here,  $\eta$ ,  $\chi$ ,  $\mu$ ,  $\omega$ , and  $S$  were calculated using the following equations [21-23]: The results are listed in Table 4, along with the total electronic densities of states (DOSs) presented in Figure 4. The data reveals a high  $E_{\text{HOMO}}-E_{\text{LUMO}}$  energy gap and a low global hardness, which indicates the low reactivity and high kinetic stability of nelarabine.

$$\begin{aligned}\eta &= I-A/2 \\ \chi &= I + A/2 \\ \mu &= -(I + A)/2 \\ \omega &= \mu^2/2\eta \\ S &= 1/2\eta\end{aligned}$$



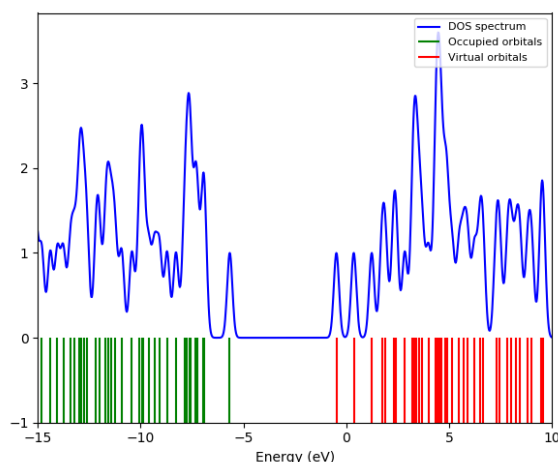


**Figure 4.** Calculated DOS plot of Nelarabine.

**Table 4.** Calculated electrical parameters of Nelarabine.

Property	Calculated value
Dipole moment (Debye)	3.0821
EHOMO (eV)	-5.67
ELUMO (eV)	-0.48
E <sub>g</sub> (eV)	5.19
I (eV)	5.67
A (eV)	0.48
χ (eV)	3.07
η (eV)	2.59
μ (eV)	-3.07
ω (eV)	1.82
S (eV)	0.19

### 3.6. QTAIM, ELF, and LOL analyses.

QTAIM was conducted to determine the nature of the chemical bonding in nelarabine at selected bond critical points (BCP). The topological parameters and molecular graph containing BCP are listed and illustrated in Table 5 and Figure 5, respectively. The topological parameters include electron density  $p(r)$ , which describes the strength of a chemical bond, the Laplacian electron density  $\nabla^2 p(r)$ , which determines where the electronic charge is locally concentrated or depleted, the electronic energy density  $H(r)$ , which is defined as the sum of the kinetic and potential energy densities ( $G(r)$  and  $V(r)$ , respectively). High positive values of  $p(r)$  indicate a stronger bond. Negative values of  $\nabla^2 p(r)$  and  $H(r)$  indicate covalent bonding, and positive values indicate non-covalent bonding. The ratio of  $V(r)$  to  $G(r)$  determines the nature of the interactions, where  $-V(r)/G(r) < 1$  indicates weak interactions [24]. The results reveal three hydrogen bonds in nelarabine with low  $p(r)$ , positive  $\nabla^2 p(r)$  values, and  $-V(r)/G(r) < 1$  between N18-H26, O10-H31, and O7-H29, which are listed in terms of decreasing strength. Moreover, the average calculated  $p(r)$  value of the O-H bonds (0.34229 a.u.) is greater than that of the N-H (0.33085 a.u.), C-N (0.32654 a.u.), and C-O bonds (0.26529 a.u.), indicating the higher strength of O-H bonds relative to other bonds. The average calculated  $\nabla^2 p(r)$  value of the O-H bonds (-1.77640 a.u.) is greater than the N-H (-1.65604 a.u.), C-N (-1.04440 a.u.), and C-O bonds (-0.49289 a.u.), indicating a higher average concentration of atomic charge along the bond path in O-H bonds relative other bonds in nelarabine. The average calculated  $-V(r)/G(r)$  value of the N-H bonds (11.23230) is greater than that of the O-H (8.94706), C-N (3.19973), and C-O bonds (2.49969), indicating that the N-H bonds exhibit stronger interactions than the other bonds in nelarabine and are more stable than the stronger O-H bonds. The strongest individual covalent bond in nelarabine is the C11-N12 bond,  $p(r) = 0.37070$  a.u.,

because of the increased confinement of  $\pi$  electrons between the two atoms. In contrast, the weakest bond is the O20-C21 bond because of its proximity to an electron-withdrawing moiety and its lack of conjugation.

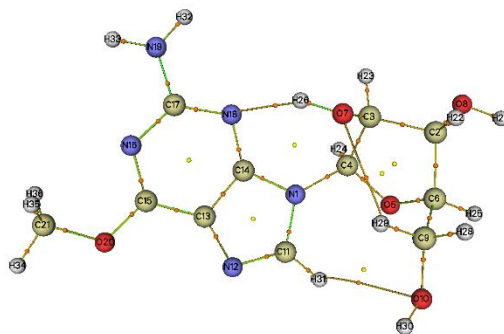


**Figure 5.** Molecular graph of Nelarabine.

**Table 5.** Calculated Topological parameters (in a.u.) at the BCPs of selected bonds in Nelarabine.

Bond	$\rho(r)$	$\nabla^2\rho(r)$	$H(r)$	$-V(r)/G(r)$	ELF	LOL
N1-C4	0.25561	-0.71482	-0.29693	3.51156	0.86207	0.71431
N1-C11	0.29737	-0.78798	-0.45296	2.76963	0.68832	0.59777
N1-C14	0.31336	-0.87905	-0.48730	2.82143	0.70650	0.60808
C2-O8	0.25775	-0.51950	-0.36280	2.55758	0.62344	0.56270
C3-O7	0.26952	-0.57161	-0.38970	2.57903	0.63120	0.56678
C4-O5	0.27366	-0.64016	-0.39577	2.67891	0.66373	0.58420
O5-C6	0.24855	-0.48681	-0.33856	2.56122	0.62856	0.56539
O7-H26	0.33195	-1.73369	-0.49557	8.97453	0.98183	0.88028
O8-H27	0.34707	-1.79173	-0.51290	8.89500	0.98287	0.88339
C9-O10	0.25716	-0.50539	-0.36290	2.53411	0.61436	0.55796
O10-H30	0.34784	-1.80376	-0.51562	8.97166	0.98314	0.88422
C11-N12	0.37070	-1.09679	-0.63098	2.76853	0.70324	0.60621
N12-C13	0.31743	-1.00399	-0.42359	3.45431	0.85791	0.71076
C14-N18	0.34355	-1.18539	-0.52385	3.30263	0.81894	0.68019
C15-N16	0.35601	-1.23712	-0.57010	3.18577	0.79487	0.66314
C15-O20	0.30966	-0.38556	-0.49094	2.24431	0.51546	0.50774
N16-C17	0.34011	-1.19292	-0.50309	3.45581	0.84361	0.69904
C17-N18	0.34760	-1.21717	-0.53614	3.31247	0.81912	0.68032
C17-N19	0.32370	-1.12880	-0.48161	3.41519	0.82840	0.68724
N19-H32	0.33077	-1.65412	-0.45857	11.18193	0.99026	0.90979
N19-H33	0.33094	-1.65796	-0.45914	11.28268	0.99044	0.91056
O20-C21	0.24072	-0.34182	-0.33484	2.34266	0.53490	0.51748
O7-H29	0.00969	0.03474	0.00093	0.87981	0.02586	0.14026
O10-H31	0.00492	0.02052	0.00112	0.71909	0.01028	0.09269
N18-H26	0.02953	0.08629	-0.00085	1.03803	0.11534	0.26537
C-N average	0.32654	-1.04440	-0.49065	3.19973	0.79230	0.66471
C-O average	0.26529	-0.49298	-0.38222	2.49969	0.60166	0.55175
N-H average	0.33085	-1.65604	-0.45885	11.23230	0.99035	0.91018
O-H average	0.34229	-1.77640	-0.50803	8.94706	0.98261	0.88263

The electron localization function (ELF) and localized orbital locator (LOL) analyses of nelarabine were performed; the results are summarized in Table 5 and illustrated for the planar modified purine moiety (Figure 6). The ELF and LOL are visual descriptors that provide a visual representation of electron pair localization concerning a reference electron in a system in terms of a scalar field, with values ranging from 0 (blue) to 1 (red); higher values indicate perfect localization and lower values suggest electron gas-like behavior [25]. Bonding types can be distinguished from the ELF and LOL contour maps as well: the  $\sigma$  bond is oval, and the  $\pi$  bond is more extended or stretched perpendicular to the bond. Table 5 and Figure 6 data indicate that the electron pair localization is higher for the  $\sigma$  bonds between N-H and C-H and lone pairs than for  $\pi$  bonds on the planar modified purine moiety. However, the extent of  $\pi$  character on all other atoms suggests a high level of conjugation throughout the modified

purine moiety, which implies that preferable electronic transitions (CT) occur within the moiety relative to transitions from or toward the moiety.

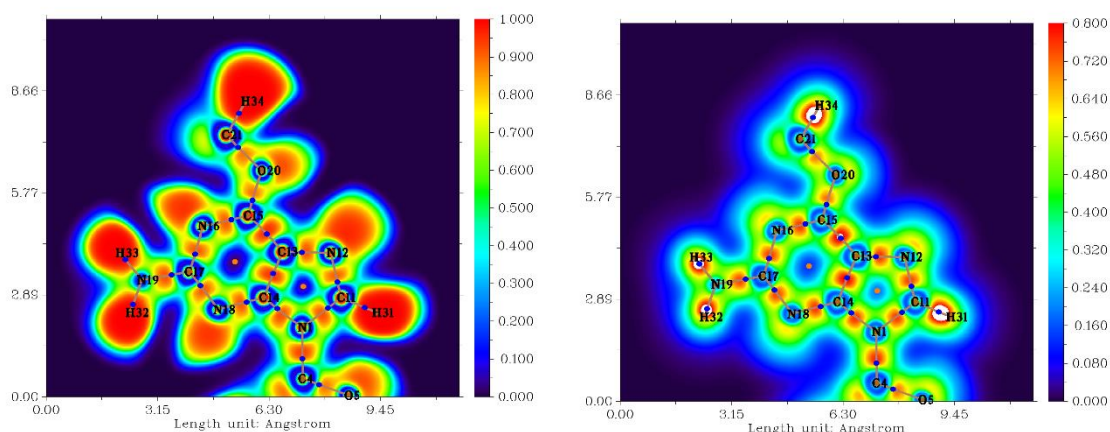


**Figure 6.** ELF and LOL plots of selected interactions within the modified purine moiety of Nelarabine.

### 3.7. Natural charge analysis.

Considering that atomic charges determine many properties of molecular systems, the natural charges of nelarabine were computed by NBO analysis and are listed in Table 6. The carbon atoms on the modified purine moiety have positive and negative charges. Carbons C11, C14, C15, and C17, which are bonded to two or three electron-withdrawing nitrogen or oxygen atoms, have positive charges. Carbons C13 and C21, bonded to one electron-withdrawing nitrogen or oxygen atom, have negative charges. The most positively charged carbon atom in the modified purine moiety is C17 (0.61339), bonded to three electron-withdrawing nitrogen atoms. The most negatively charged carbon atom in the modified purine moiety is methyl C21 (-0.32346), bonded to one electron-withdrawing oxygen atom. Nitrogen and oxygen atoms in the modified purine moiety are negatively charged, with N19 (-0.83245) being the most negatively charged and N12 (-0.46842) being the least negatively charged atom among the nitrogen and oxygen atoms in the moiety. All carbon atoms on the sugar moiety are bonded to electron-withdrawing atoms and have positive and negative charges. Carbons C2, C3, C4, and C6 are bonded to one hydrogen atom and have positive charges, whereas C9 (-0.13051) is bonded to two hydrogen atoms and has a negative charge. The most positively charged carbon atom in the sugar moiety is C4 (0.25642), bonded to two electron-withdrawing nitrogen and oxygen atoms. Oxygen atoms in the sugar moiety have negative charges, with O7 (-0.77778) being the most negatively charged and O5 (-0.57932) the least negatively charged atom. All hydrogen atoms in nelarabine have positive charges, with H26 (0.50663) bonded to O7 on the sugar moiety being the most positively charged hydrogen atom and H28 (0.20155) bonded to C9 on the sugar moiety being the least positively charged hydrogen atom. Our natural charge analysis results agree with the findings of the MEP maps regarding the sites of susceptibility to electrophilic and nucleophilic attacks.

**Table 6.** NBO charges of Nelarabine.

Atom	Charge	Atom	Charge
N1	-0.44404	N19	-0.83245
C2	0.06095	O20	-0.49946
C3	0.05194	C21	-0.32346
C4	0.25642	H22	0.23447
O5	-0.57932	H23	0.24087
C6	0.03508	H24	0.24376
O7	-0.77778	H25	0.24315

Atom	Charge	Atom	Charge
O8	-0.75305	H26	0.50663
C9	-0.13051	H27	0.47705
O10	-0.75656	H28	0.20155
C11	0.21799	H29	0.22372
N12	-0.46842	H30	0.48139
C13	-0.01958	H21	0.25148
C14	0.384	H32	0.4139
C15	0.60217	H33	0.41687
N16	-0.61339	H34	0.22649
C17	0.61958	H35	0.21967
N18	-0.62911	H36	0.21803

### 3.8. NBO analysis.

NBO analysis was conducted to study the interactions between orbitals to obtain information regarding intramolecular CT, conjugation, hyperconjugation, and delocalization of the electron density. The calculated parameters, including occupation numbers, polarization coefficient values, intramolecular donor-acceptor interactions, and stabilization energies of selected bonds of nelarabine, are presented in Table S1-S2 (Supplementary Material).

Nelarabine displays greater conjugative and hyper conjugative electron transfer on the modified purine moiety than on the sugar moiety. The most stabilizing interactions in nelarabine are the high occupancy  $n \rightarrow \pi^*$  transitions on the modified purine moiety, with the most significant interactions occurring between n2-O20 and  $\pi^*$ -C15-N16 (51.24 kcal/mol), n1-N19 and  $\pi^*$ -C17-N18 (51.13 kcal/mol), n1-N1 and  $\pi^*$ -C13-C14 (43.26 kcal/mol), and n1-N1 and  $\pi^*$ -C11-N12 (43.17 kcal/mol). The second most stabilizing interactions are the high occupancy  $\pi \rightarrow \pi^*$  transitions on the modified purine moiety, with the most significant interactions occurring between  $\pi$ -C15-N16 and  $\pi^*$ -C17-N18 (40.96 kcal/mol),  $\pi$ -C13-C14 and  $\pi^*$ -C15-N16 (36.69 kcal/mol),  $\pi$ -C17-N18 and  $\pi^*$ -C13-C14 (32.64 kcal/mol),  $\pi$ -C11-N12 and  $\pi^*$ -C13-C14 (20.55 kcal/mol), and  $\pi$ -C13-C14 and  $\pi^*$ -C11-N12 (16.03 kcal/mol). The third most stabilizing interactions are the lower occupancy  $n \rightarrow \sigma^*$  transitions throughout the molecule, with the most significant interactions occurring between n1-N16 and  $\sigma^*$ -C17-N18 (12.78 kcal/mol), n2-O5 and  $\sigma^*$ -N1-C4 (12.27 kcal/mol), n1-N18 and  $\sigma^*$ -N16-C17 (11.82 kcal/mol), and n2-O7 and  $\sigma^*$ -C3-C4 (10.81 kcal/mol). The fourth most stabilizing transitions are the lower occupancy hyper conjugative  $\sigma \rightarrow \sigma^*$  transitions throughout the molecule, with the most significant interactions primarily occurring on the modified purine moiety between  $\sigma$ -C11-N12 and  $\sigma^*$ -C13-C15 (5.75 kcal/mol),  $\sigma$ -N1-C11 and  $\sigma^*$ -C14-N18 (5.27 kcal/mol),  $\sigma$ -C13-C14 and  $\sigma^*$ -N1-C4 (4.61 kcal/mol),  $\sigma$ -N12-C13 and  $\sigma^*$ -C11-H31 (4.50 kcal/mol),  $\sigma$ -C13-C14 and  $\sigma^*$ -C15-O20 (4.35 kcal/mol),  $\sigma$ -N19-H32 and  $\sigma^*$ -C17-N18 (4.23 kcal/mol),  $\sigma$ -C14-N18 and  $\sigma^*$ -C17-N19 (4.12 kcal/mol), and  $\sigma$ -N19-H33 and  $\sigma^*$ -N16-C17 (4.03 kcal/mol). The least stabilizing transitions are the lower occupancy hyper conjugative  $\sigma \rightarrow \pi^*$  and  $\pi \rightarrow \sigma^*$  transitions on the modified purine moiety and between the sugar and modified purine moieties. The most significant interactions are between  $\pi$ -C17-N18 and  $\sigma^*$ -O7-H26 (2.52 kcal/mol),  $\sigma$ -N19-H32 and  $\pi^*$ -C17-N18 (0.79 kcal/mol),  $\sigma$ -N19-H33 and  $\pi^*$ -C17-N18 (0.65 kcal/mol), and  $\sigma$ -O7-H26 and  $\pi^*$ -C17-N18 (0.57 kcal/mol). The interaction between C17-N18 and O7-H26 contributes to stabilizing the hydrogen bond between N18 and H26, which coincided with the findings of the QTAIM analysis, revealing the high strength of the N18-H26 hydrogen bond.

The size of the polarization coefficients of the two-hybrid orbitals from atoms A and B demonstrates their importance in bond formation. The fraction of the hybrid orbital character between hybrids A and B, the fraction of the p character, and the non-bonding and bonding to antibonding interactions provide information about the overall bond character and strength and

intramolecular CT [26,27]. Determining the order of individual bonds in terms of strength through quantitative analysis was difficult due to the significant number of conjugative and hyper conjugative interactions that strengthen or weaken some bonds. Thus, the hybrid character, the polarization of hybrid orbitals, and p character were used qualitatively to predict the bond strength. The oxygen atoms in nelarabine have the highest individual hybrid character and polarization coefficients in their O-H bonds, followed by nitrogen in N-H bonds, oxygen in C-O bonds, nitrogen in C-N bonds, and carbon in C-C bonds, indicating the importance of oxygen and nitrogen for bond formation. Among the carbon atoms bonded to either oxygen or nitrogen in nelarabine, the carbon atoms with the highest p character are C6 in O5-C6 ( $sp^{2.51}-sp^{4.37}$ ) and C21 in O20-C21 ( $sp^{2.61}-sp^{4.13}$ ), which suggests that both bonds are the weakest among the C-N and C-O bonds. In contrast, the carbon atoms with the lowest p character are C11 in C11-N12 ( $sp^{1.86}-sp^{1.88}$ ), C17 in C17-N18 ( $sp^{1.86}-sp^{1.90}$ ) C17 in N16-C17 ( $sp^{1.88}-sp^{1.89}$ ), C14 in C14-N18 ( $sp^{1.89}-sp^{1.90}$ ), and C15 in C15-N16 ( $sp^{1.93}-sp^{1.81}$ ). This suggests that the five bonds are the strongest among the C-N and C-O bonds, which parallels the findings of QTAIM analysis.

### 3.9. NLO properties.

Considering the conjugation and hyperconjugation exhibited by nelarabine, NLO analysis was performed to verify its feasibility for optoelectronic and photonic applications by studying the polarizabilities and hyperpolarizabilities. The total static dipole moment ( $\mu$ ), mean polarizability ( $\alpha$ ), anisotropy of polarizability ( $\Delta\alpha$ ), and mean first-order hyperpolarizability ( $\beta$ ) of nelarabine were estimated. The x, y, and z components of  $\mu$ ,  $\alpha$ , and  $\beta$  were used to extract the values of interest using the following equations [28-30]:

$$\mu = \sqrt{\mu_x^2 + \mu_y^2 + \mu_z^2}$$

$$\alpha = \frac{\alpha_{xx} + \alpha_{yy} + \alpha_{zz}}{3}$$

$$\Delta\alpha = \frac{1}{\sqrt{2}} \sqrt{(\alpha_{xx} - \alpha_{yy})^2 + (\alpha_{yy} - \alpha_{zz})^2 + (\alpha_{zz} - \alpha_{xx})^2 + 6(\alpha_{xy}^2 + \alpha_{yz}^2 + \alpha_{xz}^2)}$$

$$\beta_x = \beta_{xxx} + \beta_{xyy} + \beta_{xzz}$$

$$\beta_y = \beta_{yyy} + \beta_{xxy} + \beta_{yzz}$$

$$\beta_z = \beta_{zzz} + \beta_{xxz} + \beta_{yyz}$$

$$\beta = \sqrt{\beta_x^2 + \beta_y^2 + \beta_z^2}$$

The results of NLO analysis are summarized in Table 7 and compared with those of urea as a reference standard. Nelarabine exhibits moderate  $\beta$  values, which were 2.59 times higher than those of urea ( $\mu = 1.3732$  Debye,  $\beta = 0.3728 \times 10^{-30}$  esu) [28]. The results confirm that nelarabine can be used in optoelectronic applications with low efficiency. However, this finding suggests that the optoelectronic applicability of nelarabine could be drastically improved with further modifications to the purine and sugar moieties that enhance the donor-acceptor interactions between the moieties.



**Table 7.** NLO parameters of Nelarabine.

Parameter	Calculated value
<b>Dipole moment (<math>\mu</math>) Debye</b>	
$\mu_x$	-0.2536
$\mu_y$	2.8465
$\mu_z$	1.1536
M	3.0818
<b>Polarizability (<math>\alpha</math>) <math>\times 10^{-24}</math> esu</b>	
$\alpha_{xx}$	32.8551
$\alpha_{xy}$	-0.6874
$\alpha_{yy}$	24.9718
$\alpha_{xz}$	-1.6974
$\alpha_{yz}$	0.5774
$\alpha_{zz}$	14.7822
A	24.2030
$\Delta\alpha$	16.0425
<b>Hyperpolarizability (<math>\beta</math>) <math>\times 10^{-30}</math> esu</b>	
$\beta_{xxx}$	0.3745
$\beta_{xxy}$	-1.0786
$\beta_{xyy}$	-0.9468
$\beta_{yyy}$	0.9486
$\beta_{xxz}$	-0.4035
$\beta_{xyz}$	-0.2132
$\beta_{yyz}$	0.3415
$\beta_{xzz}$	-0.2791
$\beta_{yzz}$	-0.1410
$\beta_{zzz}$	-0.3046
$\beta_x$	-0.8514
$\beta_y$	-0.2710
$\beta_z$	-0.3666
B	0.9658

### 3.10. Thermodynamic properties.

The thermodynamic parameters, including zero-point vibrational energy, thermal energy, specific heat capacity, rotational constant, entropy, and dipole moment of nelarabine, were calculated at 298.15 K and 1 atm; the results are listed in Table 8. The calculated standard thermodynamic values can be used to calculate the changes in heat capacity, enthalpy, and entropy in a reaction.

**Table 8.** Calculated Thermodynamical parameters of Nelarabine.

Thermodynamic Parameters	Calculated value
SCF energy(a.u.)	-1078.049
Total thermal energy(Kcal/mol)	190.809
Vibrational energy(Kcal/mol)	189.032
Zero point vibrational energy(Kcal/mol)	178.88
Heat capacity Cv(cal/mol-Kelvin)	72.671
Entropy(cal/mol-Kelvin)	141.359
<b>Rotational Constants(GHz)</b>	
Along X-direction	0.61777
Along Y-direction	0.19516
Along Z-direction	0.1614

### 3.11. Pharmacological investigation.

The applicability of molecules as potential drugs generally satisfies Lipinski's rule of five [31]. The physicochemical, lipophilicity, water solubility, and drug-likeness parameters of nelarabine were calculated using SwissADME; the results are summarized in Table 9. The bioavailability radar, which reflects the suitable physicochemical space for oral bioavailability, was calculated by SwissADME and illustrated in Figure 7. The pharmacokinetic profile parameters are based on absorption, distribution, metabolism, and excretion (ADME), which

include human intestinal absorption (HIA), blood-brain barrier penetration (BBB), P-glycoprotein (P-gp) inhibitor and substrate, CYP1A2 inhibitor, CYP2C19 inhibitor, CYP2C9 inhibitor, CYP2D6 inhibitor, CYP2D6 substrate, CYP3A4 inhibitor, CYP3A4 substrate, skin permeability (LogKp), the permeability of Madin-Darby canine kidney cells (MDCK cells), plasma protein binding, and CaCO-2 cell permeability, were calculated using Pre-ADMET and SwissADME [32,33]; the results are summarized in Table 10. The sites of metabolism by cytochrome P450 were predicted by SOMP; the results are presented in Table 11 and Figure 8. The pharmacodynamic profile parameters, including pharmacological activities and adverse reactions, were calculated using PASSOnline; the results are listed in Tables S3-S4. In addition, the cancer cell line cytotoxicity, organ toxicity, and related side effects were calculated using CLC-Pred and MetaTox, respectively; the results are summarized in Tables 12-13.

The results in Table 9 indicate that nelarabine satisfies Lipinski's rule for drug-likeness, with an oral bioavailability of 55% and that it displays favorable physicochemical properties, including high water solubility and good acid-base character because it has more hydrogen bond acceptors (8) than donors (4). Nelarabine had an adequate lipophilicity (cLogP) value (-1.35) and a high topological polar surface area (TPSA) value (148.77 Å<sup>2</sup>), which indicates low cell permeability. Therefore, the bioavailability was considered limited, as illustrated in Figure 7, where nelarabine is not totally confined in the suitable physicochemical space for oral bioavailability.

**Table 9.** Physicochemical profile and drug-likeness of Nelarabine.

Physicochemical parameters	
Formula	C11H15N5O5
Molecular weight	297.27 g/mol
Num. heavy atoms	21
Num. arom. heavy atoms	9
Fraction Csp3	0.55
Num. rotatable bonds	3
Num. H-bond acceptors	8
Num. H-bond donors	4
Molar Refractivity	69.17
TPSA	148.77 Å <sup>2</sup>
Lipophilicity	
Log Po/w (iLOGP)	1.04
Log Po/w (XLOGP3)	-1.03
Log Po/w (WLOGP)	-2.29
Log Po/w (MLOGP)	-2.12
Log Po/w (SILICOS-IT)	-2.36
Consensus Log Po/w	-1.35
Water Solubility	
Log S (ESOL)	-1.15
Solubility	2.09e+01 mg/ml ; 7.03e-02 mol/l
Class	Very soluble
Log S (Ali)	-1.61
Solubility	7.36e+00 mg/ml ; 2.47e-02 mol/l
Class	Very soluble
Log S (SILICOS-IT)	0.29
Solubility	5.82e+02 mg/ml ; 1.96e+00 mol/l
Class	Soluble
Drug-likeness	
Lipinski	Yes; 0 violation
Ghose	No; 1 violation: WLOGP<-0.4
Veber	No; 1 violation: TPSA>140
Egan	No; 1 violation: TPSA>131.6
Muegge	Yes
Bioavailability Score	0.55

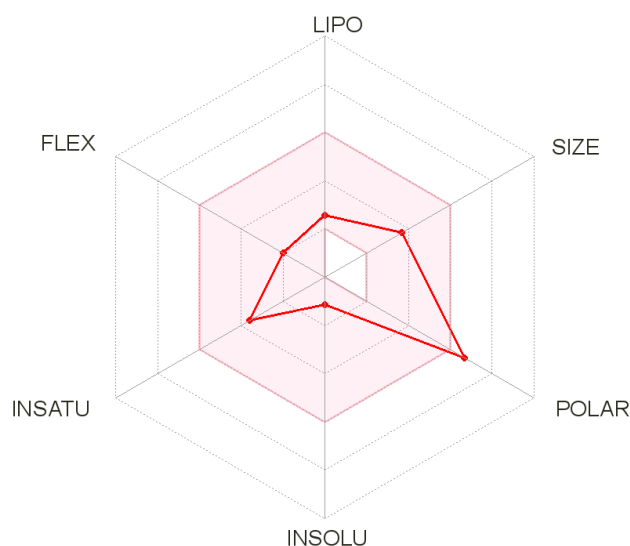


**Figure 7.** Oral bioavailability radar of nelarabine. Bioavailability radar (pink area exhibits optimal range of particular property) for studied compounds [LIPO = lipophilicity as XLOGP3; SIZE = size as molecular weight; POLAR = polarity as TPSA (topological polar surface area); INSOLU = insolubility in water by log *S* scale; INSATU = insaturation *as per* fraction of carbons in the  $sp^3$  hybridization and FLEX = flexibility *as per* rotatable bonds].

The analysis of the pharmacokinetic profile of nelarabine presented in Table 10 reveals moderate HIA (20%–70%), no BBB penetration (less than 0.4), low MDCK (<25 nm/s), and moderate CaCO-2 (4–70 nm/s) cell permeability, which are attributed to the physicochemical properties and thereby affirming its low potential to become an oral drug. In addition, P-gp is overexpressed in cancer cells and is responsible for drug efflux in tumors. Nelarabine does not inhibit P-gp, indicative of limited bioavailability and anti-tumor activity [34]. Moreover, nelarabine exhibited weak plasma protein binding (<90%), suggesting swift exertion, strong pharmacological effects, and strong interactions with the targets. Nelarabine also exhibits a negative LogKp value, which corresponds to skin impermeability. Furthermore, the computed metabolism parameters indicate that nelarabine is a weak substrate of CYP3A4 while no inhibition was evident for all the listed cytochrome P450 members in the SwissADME results; However, inhibition of CYP3A4 was observed in the Pre-ADMET results. This suggests appropriate metabolism by the cytochrome P450 members and the possibility of drug-drug interactions with CYP3A4. Moreover, regarding the sites of metabolism by cytochrome P450, C9 (9) and C21 (25) were determined to be the main sites for *O*-phosphorylation by cytochrome P450 members (Table 11, Figure 8), in which nelarabine is converted to ara-GTP.

**Table 10.** Pharmacokinetic profile of Nelarabine.

Pharmacokinetic profile	SwissADME	Pre-ADMET
HI absorption	Low	40.9985%
BBB penetration	No	0.01245
P-gp substrate	No	-
P-gp inhibitor	-	No
CYP1A2 inhibitor	No	-
CYP2C19 inhibitor	No	No
CYP2C9 inhibitor	No	No
CYP2D6 inhibitor	No	No
CYP2D6 substrate	-	No
CYP3A4 inhibitor	No	Yes
CYP3A4 substrate	-	Weak
Log Kp (skin permeation)	-8.84 cm/s	-5.16202 cm/hr
MDCK cell permeability	-	0.63508 nm/s
CaCo2 cell permeability	-	13.7711 nm/s
Plasma protein binding	-	12.08715%

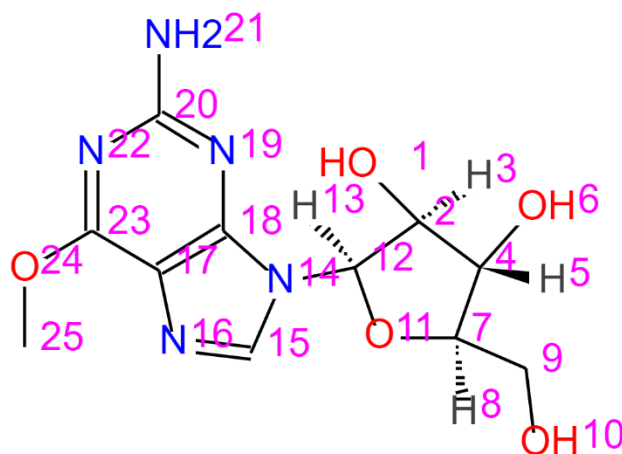


**Figure 8.** Atom numbering of metabolic sites.

**Table 11.** Main metabolic sites on Nelarabine by cytochrome P450 members.

CYP3A4		CYP2D6		CYP2C19		CYP2C9		CYP1A2	
Atom number	Probability	Atom number	Probability	Atom number	Probability	Atom number	Probability	Atom number	Probability
25	0,404	25	0,723	25	0,620	9	0,803	9	0,666
15	0,351	9	0,486	9	0,416	25	0,648	25	0,515
9	0,162	15	0,440	4	0,313	3	0,323	12	0,441
3	0,080	3	0,295	2	0,205	5	0,323	15	0,329
5	0,080	5	0,295	12	0,203	8	0,323	4	0,186
8	0,080	8	0,295	3	0,074	13	0,323	3	0,093
13	0,080	13	0,295	5	0,074	4	0,276	5	0,093
14	-0,930	12	0,219	8	0,074	21	0,198	8	0,093
11	-0,848	4	0,122	13	0,074	2	0,191	13	0,093
17	-0,783	7	0,071	16	0,029	12	0,169	2	0,037
19	-0,774	2	0,068	24	-0,773	14	0,167	21	0,014
23	-0,730	19	-0,850	19	-0,771	7	0,162	14	-0,909
1	-0,697	14	-0,846	22	-0,738	16	0,119	20	-0,851
6	-0,694	17	-0,825	21	-0,640	10	0,079	17	-0,833
18	-0,641	23	-0,797	1	-0,605	11	0,064	19	-0,833
24	-0,634	24	-0,693	6	-0,605	17	-0,908	23	-0,820
20	-0,628	16	-0,681	10	-0,598	23	-0,904	18	-0,769
10	-0,613	22	-0,667	20	-0,540	18	-0,848	16	-0,675
22	-0,613	20	-0,625	11	-0,493	20	-0,833	22	-0,593
21	-0,581	18	-0,591	23	-0,434	19	-0,740	24	-0,589
7	-0,536	21	-0,505	14	-0,210	15	-0,617	1	-0,341
12	-0,530	1	-0,275	17	-0,172	22	-0,595	6	-0,341
16	-0,451	6	-0,275	7	-0,093	24	-0,523	10	-0,309
2	-0,450	10	-0,244	15	-0,068	1	-0,215	11	-0,251
4	-0,356	11	-0,137	18	-0,040	6	-0,215	7	-0,016

The pharmacodynamic profile of nelarabine presented in Tables 12-13 and S3-S4 (Supplementary Material) reveals many pharmacological activities, in addition to high anti-tumor activity, antiviral activity, carcinogenicity, mutagenicity, and severe adverse reactions. Among the most probable pharmacological activities were antiviral activities against poxvirus, herpes, and picornavirus (Table S3). In addition, nelarabine exhibits a high probability of cytostatic, antineoplastic, and antimetabolite activity through destructive interactions with DNA, which suggests anticancer, carcinogenic, mutagenic, and reproductive effects (Table 12). However, it exhibits selectivity for attacking tumor cells relative to non-tumor cells while displaying high anticancer activity against childhood T-cell acute lymphoblastic leukemia (CCRF-CEM), lung adenocarcinoma (PC-9), promyeloblast leukemia (HL-60), childhood acute myeloid leukemia with maturation (Kasumi 1), non-small cell lung carcinoma (NCI-H23), and non-small cell lung cancer stage 3 (NCI-H838). Anticancer activity against glioblastoma (SNB-7) is listed; however, due to poor BBB penetration, this activity should be

ignored for nelarabine but not for ara-GTP [35] (Table 13). Analogous to almost all anticancer drugs, nelarabine displays possible severe adverse reactions (Table S4), which include sweating, diarrhea, inflammation, headache, nausea, pain, acidosis, hyperuricemia, splenomegaly, stomatitis, ototoxicity, agranulocytosis, thrombocytopenia, leukopenia, anemia, respiratory failure, coma, and several other probable adverse reactions.

**Table 12.** Organ toxicity and related side effects.

Pa	Pi	Organ acute toxicity
0.853	0.005	Carcinogenic, male mice, lung
0.735	0.024	Carcinogenic, female rats, ear Zymbals gland
0.698	0.061	Carcinogenic, female mice, hematopoietic system
0.572	0.074	Carcinogenic, female mice, lung
		<b>Side Effect</b>
0.961	0.004	Mutagenicity
0.645	0.043	Reproductive Effects

Pa, the probability to be active; Pi, the probability to be inactive

**Table 13.** Tumor cell line toxicity.

Pa	Pi	Cell-line	Cell-line full name	Tissue	Tumor type
0.754	0.005	CCRF-CEM	Childhood T acute lymphoblastic leukemia	Blood	Leukemia
0.709	0	SNB-7	Glioblastoma	Brain	Glioblastoma
0.624	0.005	PC-9	Lung adenocarcinoma	Lung	Adenocarcinoma
0.569	0.02	HL-60	Promyeloblast leukemia	Hematopoietic and lymphoid tissue	Leukemia
0.537	0.026	Kasumi 1	Childhood acute myeloid leukemia with maturation	Hematopoietic and lymphoid tissue	Leukemia
0.501	0.019	NCI-H23	Non-small cell lung carcinoma	Lung	Carcinoma
0.501	0.049	NCI-H838	Non-small cell lung cancer. 3 stage	Lung	Carcinoma

Pa, the probability to be active; Pi, the probability to be inactive

#### 4. Conclusions

Nelarabine was synthesized and modeled using DFT/TD-DFT calculations (B3LYP/6-31G\* level of theory) and QSAR. The experimental and calculated IR spectral parameters were in excellent agreement. The experimental absorption spectrum in a 9:1 mixture of phosphate buffer (pH 7.0) and ethanol was in excellent agreement with the theoretical absorption spectrum calculated in ethanol. According to FMO analysis, nelarabine exhibited low reactivity and kinetic stability through a high  $E_{\text{HOMO}}-E_{\text{LUMO}}$  energy gap and low global hardness. Nelarabine demonstrated low efficiency in nonlinear optical activity according to NLO analysis. The NBO analysis conclusions paralleled the conclusions from QTAIM analysis regarding hydrogen bond stability, covalent bond stability, and the localization of intramolecular CT within the modified purine moiety. Natural charge and MEP map analyses agreed on the sites susceptible to electrophilic and nucleophilic attacks; however, they oppose the findings from QSAR models regarding the selectivity of metabolism by cytochrome P450 members. The physicochemical profile of nelarabine suggests inadequate oral bioavailability; however, because of its high solubility, intravenous administration, cytotoxicity, and antimetabolic properties, it has high potential as an anticancer and antiviral compound. According to QSAR models, Nelarabine exhibits poor BBB penetration and no P-gp inhibition, which corresponds to fewer adverse effects before being metabolized into ara-GTP—the most probable metabolic form through *O*-phosphorylation site predictions—which reportedly demonstrates improved bioavailability. The pharmacodynamic profile of nelarabine was



investigated; however, to understand the complete profile, an extensive study with the most probable metabolites, including ara-GTP, must be conducted. The QSAR models aid in drug discovery but are not conclusive regarding the drug's effectiveness. Quantum chemical findings and the known potential of modified nucleosides regarding anticancer and antiviral activities promote further research into inexpensive synthetic modification routes to discover viable anticancer and antiviral candidates, including those wherein nelarabine is the main compound.

## Funding

This research received no external funding.

## Acknowledgments

This research has no acknowledgment.

## Conflicts of Interest

The authors declare no conflict of interest.

## References

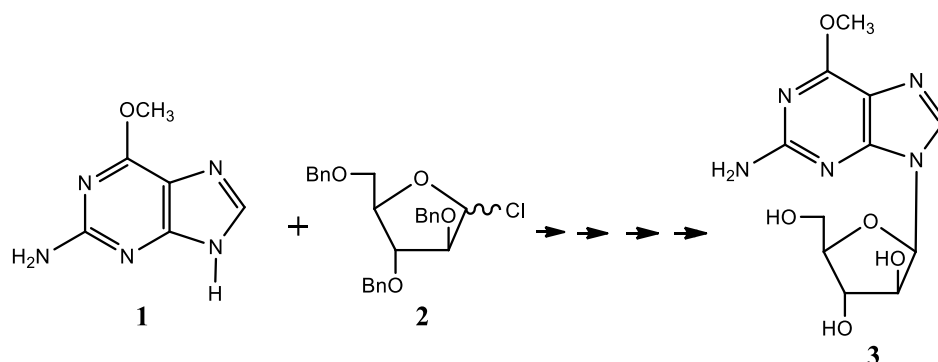
1. Arco, J.; Fernandez-Lucas, J. Purine And Pyrimidine Phosphoribosyltransferases: A Versatile Tool For Enzymatic Synthesis Of Nucleoside-5'-Monophosphates. *Current Pharmaceutical Design* **2018**, *23*, 6898-6912, <https://doi.org/10.2174/1381612823666171017165707>.
2. Averett, D.; Koszalka, G.; Fyfe, J.; Roberts, G.; Purifoy, D.; Krenitsky, T. 6-Methoxypurine Arabinoside As A Selective And Potent Inhibitor Of Varicella-Zoster Virus. *Antimicrobial Agents and Chemotherapy* **1991**, *35*, 851-857, <https://doi.org/10.1128/aac.35.5.851>.
3. Lambe, C.U.; Averett, D.; Paff, M.; Reardon, J.; Wilson, J.; Krenitsky, T. 2-Amino-6-methoxypurine arabinoside: an agent for T-cell malignancies. *Cancer research* **1995**, *55*, 3352-3356.
4. Buie, L.; Epstein, S.; Lindley, C. Nelarabine: A Novel Purine Antimetabolite Antineoplastic Agent. *Clinical Therapeutics* **2007**, *29*, 1887-1899, <https://doi.org/10.1016/j.clinthera.2007.09.002>.
5. Elion, G. The Purine Path To Chemotherapy. *Science* **1989**, *244*, 41-47, <https://doi.org/10.1126/science.2649979>.
6. Mikhailopulo, I.; Konstantinova, I.; Antonov, K.; Fateev, I.; Miroshnikov, A.; Stepchenko, V.; Baranovsky, A. A Chemo-Enzymatic Synthesis Of B-D-Arabinofuranosyl Purine Nucleosides. *Synthesis* **2011**, *2011*, 1555-1560, <https://doi.org/10.1055/s-0030-1260010>.
7. Frisch, M.J.; Trucks, G.W.; Schlegel, H.B.; Scuseria, G.E.; Robb, M.A.; Cheeseman, J.R.; Scalmani, G.V.; Barone, G.A.; Petersson, H.; Nakatsuji, X.; Li, M.; Caricato, A.; Marenich, J.; Bloino, B.G.; Janesko, R.; Gomperts, B.; Mennucci, H.P.; Hratchian, J.V.; Ortiz, A.F.; Izmaylov, J.L.; Sonnenberg, D.; Williams-Young, F.; Ding, F.; Lipparini, F.; Egidi, J.; Goings, B.; Peng, A.; Petrone, T.; Henderson, D.; Ranasinghe, V.G.; Zakrzewski, J.; Gao, N.; Rega, G.; Zheng, W.; Liang, M.; Hada, M.; Ehara, K.; Toyota, R.; Fukuda, J.; Hasegawa, M.; Ishida, T.; Nakajima, Y.; Honda, O.; Kitao, H.; Nakai, T.; Vreven, K.; Throssell, J.A.; Montgomery, Jr.J.E.; Peralta, F.; Ogliaro, M.; Bearpark, J.J.; Heyd, E.; Brothers, K.N.; Kudin, V.N.; Staroverov, T.; Keith, R.; Kobayashi, J.; Normand, K.; Raghavachari, A.; Rendell, J.C.; Burant, S.S.; Iyengar, J.; Tomasi, M.; Cossi, J.M.; Millam, M.; Klene, C.; Adamo, R.; Cammi, J.W.; Ochterski, R.L.; Martin, K.; Morokuma, O.; Farkas, J.B.; Foresman, D.J.; Fox, D.J. Gaussian, Inc., Wallingford CT, Gaussian 09, Revision D.01, **2016**.
8. Lu, T.; Chen, F. Multiwfn: A Multifunctional Wavefunction Analyzer. *Journal of Computational Chemistry* **2011**, *33*, 580-592, <https://doi.org/10.1002/jcc.22885>.
9. NBO, 7.0. Glendening, E.D.; Badenhoop, J.K.; Reed, A.E.; Carpenter, J.E.; Bohmann, J.A.; Karafiloglou, C.M.P.; Morales, C.; Landis, R.; Weinhold, F. Theoretical Chemistry Institute, University of Wisconsin, Madison, **2018**.
10. Lee, S.K.; Lee, I.H.; Kim, H.J.; Chang, G.S.; Chung, J.E.; No, K.T. The PreADME Approach: Web-based program for rapid prediction of physico-chemical, drug absorption and drug-like properties. In: *EuroQSAR 2002 Designing Drugs and Crop Protectants: Processes, Problems and Solutions*. **2003**; pp. 418-420.
11. Daina, A.; Michielin, O.; Zoete, V. Swissadme: A Free Web Tool To Evaluate Pharmacokinetics, Drug-Likeness And Medicinal Chemistry Friendliness Of Small Molecules. *Scientific Reports* **2017**, *7*, <https://doi.org/10.1038/srep42717>.

12. Filimonov, D.; Lagunin, A.; Glorizova, T.; Rudik, A.; Druzhilovskii, D.; Pogodin, P.; Poroikov, V. Prediction Of The Biological Activity Spectra Of Organic Compounds Using The Pass Online Web Resource. *Chemistry of Heterocyclic Compounds* **2014**, *50*, 444-457, <https://doi.org/10.1007/s10593-014-1496-1>.
13. Lagunin, A.; Dubovskaja, V.; Rudik, A.; Pogodin, P.; Druzhilovskiy, D.; Glorizova, T.; Filimonov, D.; Sastry, N.; Poroikov, V. CLC-Pred: A Freely Available Web-Service For In Silico Prediction Of Human Cell Line Cytotoxicity For Drug-Like Compounds. *PLOS ONE* **2018**, *13*, <https://doi.org/10.1371/journal.pone.0191838>.
14. Rudik, A.; Dmitriev, A.; Lagunin, A.; Filimonov, D.; Poroikov, V. SOMP: Web Server For In Silico Prediction Of Sites Of Metabolism For Drug-Like Compounds. *Bioinformatics* **2015**, *31*, 2046-2048, <https://doi.org/10.1093/bioinformatics/btv087>.
15. Rudik, A.; Bezhtentsev, V.; Dmitriev, A.; Druzhilovskiy, D.; Lagunin, A.; Filimonov, D.; Poroikov, V. Metatox: Web Application For Predicting Structure And Toxicity Of Xenobiotics' Metabolites. *Journal of Chemical Information and Modeling* **2017**, *57*, 638-642, <https://doi.org/10.1021/acs.jcim.6b00662>.
16. Sheikhi, M.; Shahab, S.; Alnajjar, R.; Ahmadianarog, M. Adsorption Properties Of The New Anti-Cancer Drug Alectinib On CNT(6,6-6) Nanotube: Geometry Optimization, Molecular Structure, Spectroscopic (NMR, UV/Vis, Excited State), FMO, MEP And HOMO–LUMO Investigations. *Journal of Cluster Science* **2018**, *30*, 83-96, <https://doi.org/10.1007/s10876-018-1460-9>.
17. Shamim, S.; Miah, M.; Hossain, M.; Hasan, M.; Hossain, M.; Hossain, M.; Ahmed, F. Theoretical Investigation Of Emodin Conjugated Doped B12N12 Nanocage By Means Of DFT, QTAIM And PCM Analysis. *Physica E: Low-dimensional Systems and Nanostructures* **2022**, *136*, <https://doi.org/10.1016/j.physe.2021.115027>.
18. Mittal, A.; Kakkar, R. A Theoretical Assessment Of The Structural And Electronic Features Of Some Retrochalcones. *International Journal of Quantum Chemistry* **2021**, *121*, <https://doi.org/10.1002/qua.26797>.
19. Shahab, S.; Sheikhi, M.; Filippovich, L.; Ihnatovich, Z.; Koroleva, E.; Drachilovskaya, M.; Atroshko, M.; Pazniak, A. Spectroscopic (FT-IR, Excited States, UV/Vis, Polarization) Properties, Synthesis And Quantum Chemical Studies Of New Azomethine Derivatives. *Dyes and Pigments* **2019**, *170*, <https://doi.org/10.1016/j.dyepig.2019.107647>.
20. Pandey, N.; Mehata, M.; Pant, S.; Tewari, N. Structural, Electronic And NLO Properties Of 6-Aminoquinoline: A DFT/TD-DFT Study. *Journal of Fluorescence* **2021**, *31*, 1719-1729, <https://doi.org/10.1007/s10895-021-02788-z>.
21. Shahab, S.; Almodarresiyeh, H.; Filippovich, L.; Hajikolaee, F.; Kumar, R.; Darroudi, M.; Mashayekhi, M. Geometry Optimization And Excited State Properties Of The New Symmetric (E)-Stilbene Derivative For Application In Thermostable Polarizing PVA-Films: A Combined Experimental And DFT Approach. *Journal of Molecular Structure* **2016**, *1119*, 423-430.
22. Mubarik, A.; Rasool, N.; Hashmi, M.; Mansha, A.; Zubair, M.; Shaik, M.; Sharaf, M.; Awwad, E.; Abdelgawad, A. Computational Study Of Structural, Molecular Orbitals, Optical And Thermodynamic Parameters Of Thiophene Sulfonamide Derivatives. *Crystals* **2021**, *11*, <https://doi.org/10.3390/cryst11020211>.
23. Srishailam, K.; Ramaiah, K.; Reddy, K.; Reddy, B.; Rao, G. Synthesis And Evaluation Of Molecular Structure From Torsional Scans, Study Of Molecular Characteristics Using Spectroscopic And DFT Methods Of Some Thiosemicarbazones, And Investigation Of Their Anticancer Activity. *Chemical Papers* **2021**, *75*, 3635-3647, <https://doi.org/10.1007/s11696-021-01595-x>.
24. Jenkins, S.; Morrison, I. The Chemical Character Of The Intermolecular Bonds Of Seven Phases Of Ice As Revealed By Ab Initio Calculation Of Electron Densities. *Chemical Physics Letters* **2000**, *317*, 97-102, [https://doi.org/10.1016/S0009-2614\(99\)01306-8](https://doi.org/10.1016/S0009-2614(99)01306-8).
25. Fuentealba, P.; Santos, C.J. Electron Localization Function As A Measure Of Electron Delocalization And Aromaticity. *Current Organic Chemistry* **2011**, *15*, 3619-3626, <https://doi.org/10.2174/138527211797636200>.
26. Shahab, S.; Sheikhi, M.; Kvasnyuk, E.; Sysa, A.; Alnajjar, R.; Strogova, A.; Sirotsina, K.; Yurlevich, H.; Novik, D. Geometry Optimization, UV/Vis, NBO, HOMO And LUMO, Excited State And Antioxidant Evaluation Of Pyrimidine Derivatives. *Letters in Organic Chemistry* **2021**, *18*, 465-476, <https://doi.org/10.2174/1570178617999200812133402>.
27. Isik, I.; Sagdinc, S. Theoretical (Hirshfeld Surface, Molecular Docking, Structural, Electronic Properties, NBO And NLO Analyses) And Spectroscopic Studies Of 6-Chloro-2-Oxindole In Monomeric And Dimeric Forms. *Journal of Molecular Structure* **2021**, *1245*, <https://doi.org/10.1016/j.molstruc.2021.130981>.
28. Prashanth, J.; Ramesh, G.; Naik, J.; Ojha, J.; Reddy, B.; Rao, G. Molecular Structure, Vibrational Analysis And First Order Hyperpolarizability Of 4-Methyl-3-Nitrobenzoic Acid Using Density Functional Theory. *Optics and Photonics Journal* **2015**, *05*, 91-107, <https://doi.org/10.4236/opj.2015.53008>.
29. Benmohammed, A.; Hadji, D.; Guendouzi, A.; Mouchaal, Y.; Djafri, A.; Khelil, A. Synthesis, Characterization, Linear And NLO Properties Of Novel N-(2,4-Dinitrobenzylidene)-3-Chlorobenzenamine Schiff Base: Combined Experimental And DFT Calculations. *Journal of Electronic Materials* **2021**, *2021*, <https://doi.org/10.1007/s11664-021-09046-9>.

30. Bensafi, T.; Hadji, D.; Yahiaoui, A.; Argoub, K.; Hachemaoui, A.; Kenane, A.; Baroudi, B.; Toubal, K.; Djafri, A.; Benkouider, A. Synthesis, Characterization And DFT Calculations Of Linear And NLO Properties Of Novel (Z)-5-Benzylidene-3-N(4-Methylphenyl)-2-Thioxothiazolidin-4-One. *Journal of Sulfur Chemistry* **2021**, *42*, 645-663, <https://doi.org/10.1080/17415993.2021.1951729>.
31. Lipinski, C.; Lombardo, F.; Dominy, B.; Feeney, P. Experimental And Computational Approaches To Estimate Solubility And Permeability In Drug Discovery And Development Settings. *Advanced Drug Delivery Reviews* **1997**, *23*, 3-25, [https://doi.org/10.1016/s0169-409x\(96\)00423-1](https://doi.org/10.1016/s0169-409x(96)00423-1).
32. Eslami Moghadam, M.; Jafari, A.; Kiani Khashandaragh, R.; Divsalar, A.; Ghasemzadeh, M. Three Anticancer Pt Complexes With Glycine Derivatives: Synthesis, Bioactivity On MCF-7 Cell Line, ADME Prediction, DFT, MEP, And Molecular Docking. *Journal of the Iranian Chemical Society* **2021**, *18*, 1927-1939, <https://doi.org/10.1007/s13738-021-02154-7>.
33. Flores-Holguín, N.; Frau, J.; Glossman-Mitnik, D. Computational Pharmacokinetics Report, ADMET Study And Conceptual DFT-Based Estimation Of The Chemical Reactivity Properties Of Marine Cyclopeptides. *ChemistryOpen* **2021**, *10*, 1142-1149, <https://doi.org/10.1002/open.202100178>.
34. Robinson, K.; Tiriveedhi, V. Perplexing Role Of P-Glycoprotein In Tumor Microenvironment. *Frontiers in Oncology* **2020**, *10*, <https://doi.org/10.3389/fonc.2020.00265>.
35. Kisor, D.; Reilly, K. Profile Of Nelarabine: Use In The Treatment Of T-Cell Acute Lymphoblastic Leukemia. *OncoTargets and Therapy* **2009**, *219*, <https://doi.org/10.2147/ott.s4770>.
36. Xia, R.; Sun, L.; Qu, G. Synthesis Of Nelarabine With Pure B-Anomer Through Late-Stage C-H Nitration/Nitro-Reduction. *Heterocycles* **2015**, *91*, <https://doi.org/10.3987/com-15-13350>.
37. China Patent CN 102250178 A. Int. Cl C07H1/06, C07H19/19, C07H19/167. Nov. 23, **2011**.
38. China Patent CN 103665076 A. Int. Cl C07H1/00, C07H19/19, C07H23/00. Mar. 26, **2014**.
39. Xia, R.; Sun, L. Efficient And Green Synthesis Of Purine Arabinosides Via CuO Catalyzed Dehydrazination In Tap Water. *Arkivoc* **2015**, *2015*, 284-292, <https://doi.org/10.3998/ark.5550190.p009.283>.
40. Krenitsky, T.; Koszalka, G.; Tuttle, J. Purine Nucleoside Synthesis: An Efficient Method Employing Nucleoside Phosphorylases. *Biochemistry* **1981**, *20*, 3615-3621, <https://doi.org/10.1021/bi00515a048>.
41. US Patent 5,424,295. Cl6 A61K 31/70; C07H 19/19. Jun. 13, **1995**.

## Supplementary Material

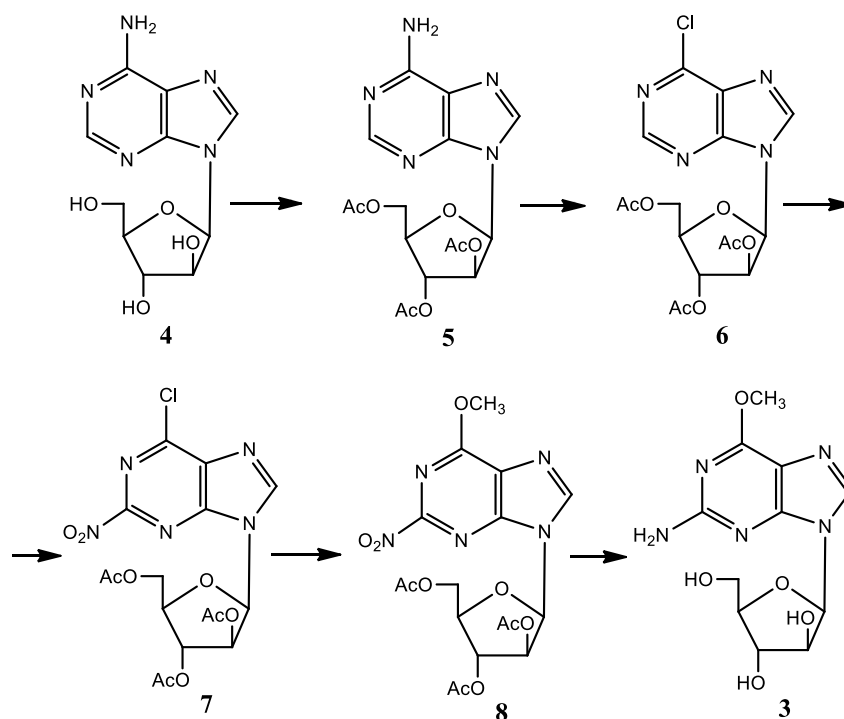
Nelarabine can be prepared via glycosylation [36]. In this case, the reaction of 2-amino-6-methoxypurine (1) with chlorosugar (2) results in the formation of nelarabine (3) and its  $\alpha$ -anomer (Scheme S1).



**Scheme S1** Synthesis of 3 by glycosylation.

However, the large-scale preparation of 3 by this method is not possible because of the difficulty in separating 3 from its  $\alpha$ -anomer.

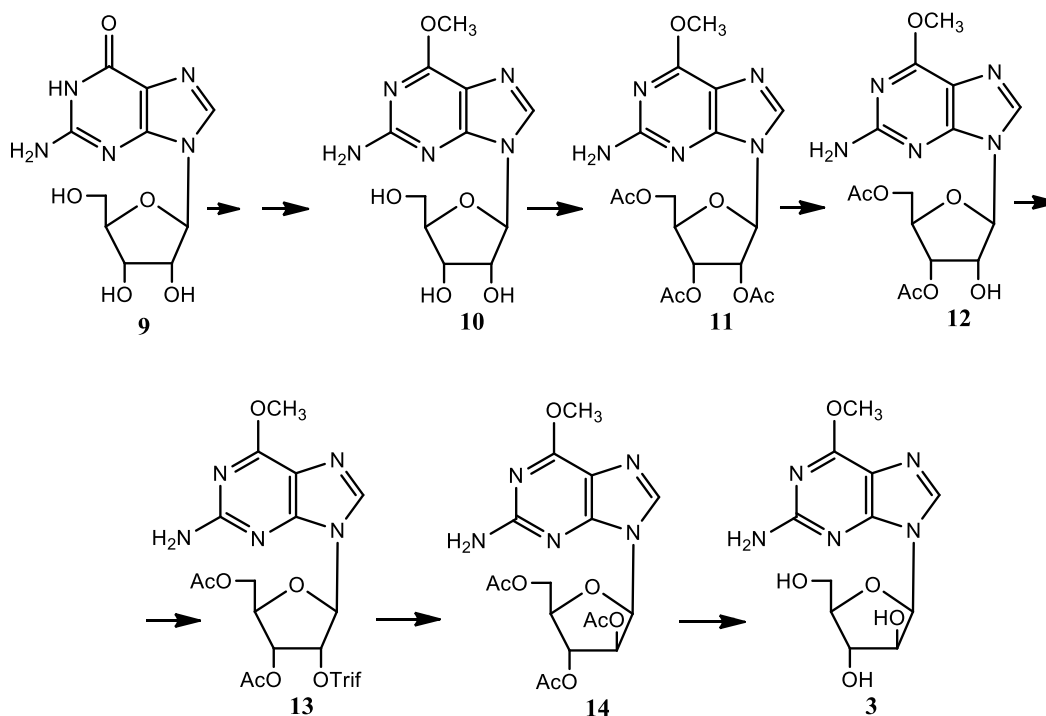
There are alternative methods for synthesizing 3, which are based on the transformation of natural and synthetic purine nucleosides. For example, the five-step transformation of commercially available arabinofuranosyladenine (araA; 4) through intermediates 5–8 results in the formation of 3 (Scheme S2) [36]. This approach for the preparation of 3 was feasible after developing the chemo-enzymatic araA synthesis route involving the use of enzymes such as nucleoside phosphorylases [37].



**Scheme S2.** Transformation of 4 to 3.

The introduction of a  $\text{CH}_3\text{O}$  group at the C-6 position of the purine moiety is an important step in synthesizing 3. The most convenient method for introducing the  $\text{CH}_3\text{O}$  group in the purine moiety is the nucleophilic displacement of chlorine in 2-amino-6-chloropurine by using sodium methylate. Guanosine (9), a natural nucleoside, is an effective starting compound

for the convenient preparation of 2-amino-6-chloropurine derivatives by protection–deprotection reactions and nucleophilic displacement, which are typically utilized in nucleoside chemistry (Scheme S3) [37].

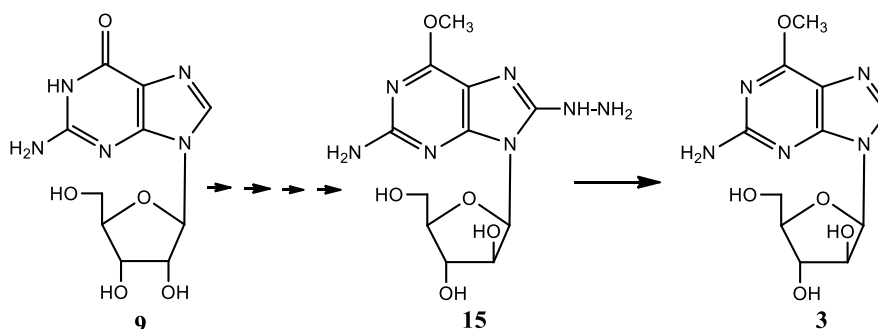


**Scheme S3.** Synthesis of 3 from 9.

The deacetylation of 11 through treatment with hydroxylamine is an inconvenient step in the transformation of 9 to 3 because of its low selectivity, which results in the formation of a mixture of 2'- and 3'-deacetylated products. The subsequent treatment of 12 with trifluoromethanesulfonic anhydride and then with acetic acid gave an acetylated derivative (14). The deacetylation of 14 through treatment with a solution of ammonia or sodium methylate in methanol afforded 3.

An analogous approach for the preparation of 3 from 9 was achieved by the same team by using 3',5'-silyl instead of acetyl protecting groups [38]. Because these approaches use inexpensive and available natural nucleosides such as 9, they are more advantageous for the preparation of 3. However, these approaches involve using expensive and toxic reagents, limiting their application for the large-scale synthesis of 3.

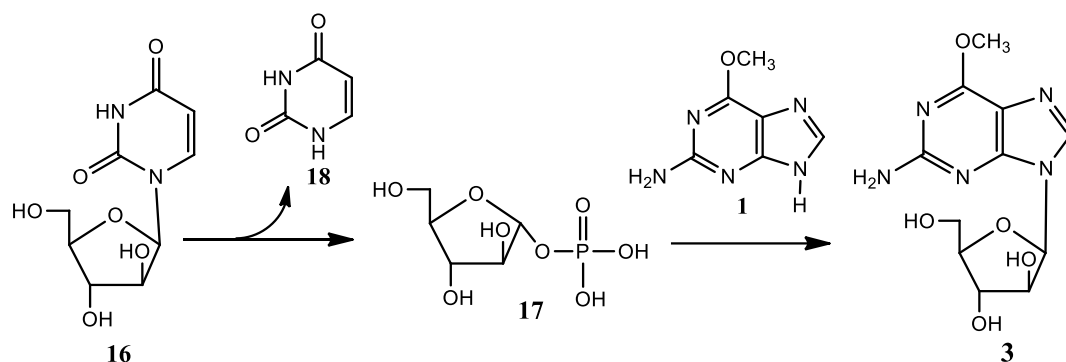
Another method for the transformation of 9 to 3 by using an 8-hydrazino derivative (15) as an intermediate (Scheme S4) has also been described [39]. Other arabinofuranoside derivatives of purines, such as fludarabine, were obtained by using the same approach.



**Scheme S4.** Synthesis of 3 from 9 through 15.



Schemes S1–S4 show that the chemical synthesis of purine arabinosides involves multiple steps and requires toxic reagents. Progress in the preparation of such nucleosides has been achieved by using bacterial phosphorylase in transglycosylation reactions [40]. This approach has also been used to synthesize **3** [41]. Arabinofuranosyluracil (**16**), which can be obtained by chemical or enzymatic deamination from commercially available arabinofuranosylcytosine (Cytosar), was used as a sugar moiety donor in the synthesis of **3**. Uridine phosphorylase transformed **16** to uracil (**18**) and arabinofuranosyl-1-phosphate (**17**) (Scheme S5). The second enzyme, purine nucleoside phosphorylase, catalyzes the glycosylation of **1** to obtain **3**.

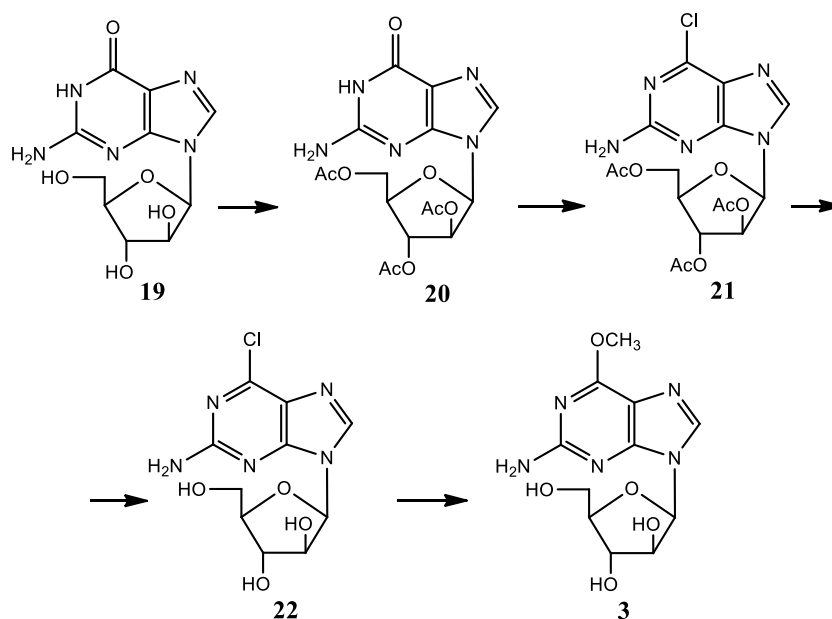


**Scheme S5.** Enzymatic synthesis of **3**.

The substrate specificity of purine nucleoside phosphorylase depends on the structure of the purine heterocycle. Therefore, some transglycosylation reactions proceed slowly and require a long time to complete. In general, this method is universal and can be used to synthesize biologically active purine arabinosides such as fludarabine [41].

Using **17** as a sugar moiety donor instead of **16** in the transglycosylation reaction also gave **3**, albeit in a low yield [6]. Furthermore, this strategy did not afford the desired product on a large scale.

Our experimental investigation aimed to develop a method to transform commercially available 9-( $\beta$ -D-arabinofuranosyl)guanine (araG; **19**) to **3** in four steps (Scheme S6).



**Scheme S6.** Synthesis of **3** from **19**.

The acetylation of 19 with acetic anhydride in acetonitrile in the presence of triethylamine and *N,N*-dimethylamine pyridine resulted in the formation of a triacetate derivative (20), which was isolated in the crystalline form with 90% yield. The treatment of 20 with a mixture of phosphor oxychloride, benzyltriethylammonium chloride, and *N,N*-dimethylaniline in acetonitrile at 100–110 °C, followed by a work-up, as described in the experimental section, gave a 6-chloro derivative (21). Compound 21, without further purification, was treated with a solution of potassium carbonate in methanol at 50–60 °C and then with Dowex 50Wx8 (H<sup>+</sup>-form, 200 mesh) to obtain deacetylated 6-chloro arabinoside (22) as an amorphous powder. To replace chlorine with a methoxy group, 22 was treated with a solution of sodium methylate in methanol, followed by neutralization with Dowex 50Wx8 (H<sup>+</sup>-form, 200 mesh). The resulting 3 was purified by SiO<sub>2</sub> column chromatography and recrystallized from water. The final yield of 3 was 43.8%.

The structure of the as-synthesized 3 was confirmed by comparison of the UV-Vis, FT-IR, and mass spectral data with a standard sample of 3.

**Table S1.** Calculated NBOs and polarization coefficients for each hybrid in selected bonds of Nelarabine (3).

Occupancy	Bond (A-B)	EDa(%)	EDb(%)	NBO	S(%) (A)	S(%) (B)	P(%) (A)	P(%) (B)
1.98519	s (N1-C4)	64.32	35.68	0.8020(sp2.01) + 0.5974(sp3.36)	33.2	22.88	66.76	76.97
1.98265	s (N1-C11)	64.8	35.2	0.8050(sp2.11) + 0.5933(sp2.44)	32.08	29.04	67.85	70.8
1.98028	s (N1-C14)	62.37	37.63	0.7897(sp1.95) + 0.6134(sp2.45)	33.86	28.98	66.07	70.91
1.99206	s (C2-O8)	33.26	66.74	0.5767(sp3.87) + 0.8170(sp2.27)	20.48	30.5	79.34	69.36
1.99283	s (C3-O7)	33.97	66.03	0.5829(sp3.61) + 0.8126(sp2.36)	21.67	29.68	78.15	70.16
1.98858	s (C4-O5)	33.11	66.89	0.5754(sp3.71) + 0.8178(sp2.52)	21.19	28.39	78.6	71.43
1.98657	s (O5-C6)	68.04	31.96	0.8249(sp2.51) + 0.5653(sp4.37)	28.42	18.57	71.43	81.23
1.98574	s (O7-H26)	76.78	23.22	0.8762(sp3.26) + 0.4819(s)	23.45	100	76.34	-
1.98883	s (O8-H27)	74.05	25.95	0.8605(sp4.04) + 0.5094(s)	19.79	100	80.02	-
1.99484	s (C9-O10)	33.34	66.66	0.5774(sp3.81) + 0.8165(sp2.38)	20.76	29.51	79.06	70.35
1.98923	s (O10-H30)	74.17	25.83	0.8612(sp4.03) + 0.5082(s)	19.85	100	79.95	-
1.98355	s (C11-N12)	40.99	59.01	0.6402(sp1.86) + 0.7682(sp1.88)	34.94	34.66	64.94	65.12
1.89373	p (C11-N12)	41.64	58.36	0.6453(sp1.00) + 0.7640(sp1.00)	0	0	99.85	99.72
1.97569	s (N12-C13)	57	43	0.7550(sp2.31) + 0.6558(sp2.09)	30.14	32.33	69.67	67.6
1.97047	s (C13-C14)	49.25	50.75	0.7018(sp2.14) + 0.7124(sp1.76)	31.81	36.26	68.12	63.69
1.6308	p (C13-C14)	56.79	43.21	0.7536(sp1.00) + 0.6573(sp1.00)	0	0.01	99.96	99.95
1.97636	s (C13-C15)	50.7	49.3	0.7120(sp1.81) + 0.7022(sp1.57)	35.62	38.84	64.33	61.11
1.98117	s (C14-N18)	41.63	58.37	0.6452(sp1.89) + 0.7640(sp1.90)	34.55	34.44	65.36	65.39
1.98432	s (C15-N16)	40.76	59.24	0.6385(sp1.93) + 0.7697(sp1.81)	34.14	35.51	65.76	64.32
1.77283	p (C15-N16)	32.45	67.55	0.5697(sp1.00) + 0.8219(sp1.00)	0	0	99.84	99.8
1.99168	s (C15-O20)	32.54	67.46	0.5705(sp2.72) + 0.8213(sp1.92)	26.83	34.18	72.98	65.66
1.98202	s (N16-C17)	59.32	40.68	0.7702(sp1.88) + 0.6378(sp1.89)	34.69	34.53	65.14	65.37
1.98167	s (C17-N18)	40.37	59.63	0.6354(sp1.86) + 0.7722(sp1.90)	34.89	34.42	65.01	65.42
1.78583	p (C17-N18)	31.39	68.61	0.5602(sp1.00) + 0.8283(sp1.00)	0	0.01	99.85	99.8
1.9909	s (C17-N19)	39.92	60.08	0.6318(sp2.29) + 0.7751(sp1.68)	30.39	37.26	69.51	62.63
1.98656	s (N19-H32)	70.85	29.15	0.8417(sp2.70) + 0.5399(s)	27.01	100	72.89	-
1.98671	s (N19-H33)	70.99	29.01	0.8426(sp2.70) + 0.5386(s)	27.11	100	72.79	-
1.99103	s (O20-C21)	68.92	31.08	0.8302(sp2.61) + 0.5575(sp4.13)	27.65	19.46	72.22	80.29
1.58373	n1(N1)	-	-	sp99.99	0.07	-	99.21	-
1.96742	n1(O5)	-	-	sp1.32	43.08	-	56.84	-
1.90485	n2(O5)	-	-	sp99.99	0.05	-	99.83	-
1.90485	n1(O7)	-	-	sp1.15	46.44	-	53.49	-
1.94507	n2(O7)	-	-	sp99.99	0.39	-	99.5	-
1.98049	n1(O8)	-	-	sp1.01	49.6	-	50.33	-
1.95816	n2(O8)	-	-	sp99.99	0.08	-	99.81	-
1.98303	n1(O10)	-	-	sp1.02	49.57	-	50.36	-
1.95946	n2(O10)	-	-	sp93.33	1.06	-	98.84	-
1.92508	n1(N12)	-	-	sp1.84	35.16	-	64.7	-
1.8899	n1(N16)	-	-	sp2.36	29.73	-	70.14	-
1.88749	n1(N18)	-	-	sp2.21	31.09	-	68.8	-
1.79524	n1(N19)	-	-	sp10.77	8.49	-	91.45	-
1.96352	n1(O20)	-	-	sp1.62	38.12	-	61.79	-
1.79468	n2(O20)	-	-	sp1.00	0	-	99.87	-

**Table S2.** Significant donor–acceptor interactions of Nelarabine (3) through second-order perturbation theory analysis of the Fock matrix

Donor(i)	Acceptor(j)	$E^{(2)a}$ (kcal/mol)	$E(j)-E(i)^b$ (a.u.)	$F(i,j)^c$ (a.u.)
n1 N 1	$\sigma^* C 3- C 4$	4.08	0.58	0.043
n1 N 1	$\sigma^* C 4- H 24$	5.61	0.72	0.057
n1 N 1	$\pi^* C 11- N 12$	43.17	0.28	0.098
n1 N 1	$\pi^* C 13- C 14$	43.26	0.28	0.099
n1 O 5	$\sigma^* C 3- C 4$	3.51	0.81	0.048
n2 O 5	$\sigma^* N 1- C 4$	12.27	0.62	0.078
n2 O 5	$\sigma^* C 6- C 9$	7.39	0.67	0.063
n1 O 7	$\sigma^* C 2- C 3$	1.57	0.85	0.033
n1 O 7	$\sigma^* C 3- H 23$	2.11	0.96	0.04
n2 O 7	$\sigma^* C 3- C 4$	10.81	0.61	0.072
n2 O 7	$\sigma^* C 3- H 23$	4.96	0.75	0.054
n1 O 8	$\sigma^* C 2- C 3$	1.46	0.88	0.032
n1 O 8	$\sigma^* C 2- C 6$	1.37	0.88	0.031
n2 O 8	$\sigma^* C 2- C 6$	6.04	0.66	0.056
n2 O 8	$\sigma^* C 2- H 22$	6.57	0.75	0.063
n1 O 10	$\sigma^* C 6- C 9$	1.02	0.89	0.027
n1 O 10	$\sigma^* C 9- H 29$	2.26	0.97	0.042
n2 O 10	$\sigma^* C 9- H 28$	7.98	0.73	0.068
n2 O 10	$\sigma^* C 9- H 29$	3.24	0.75	0.044
n1 N 12	$\sigma^* N 1- C 11$	9.88	0.73	0.076
n1 N 12	$\sigma^* C 13- C 14$	6.66	0.85	0.067
n1 N 16	$\sigma^* C 13- C 15$	9.86	0.85	0.082
n1 N 16	$\sigma^* C 15- O 20$	6.76	0.71	0.062
n1 N 16	$\sigma^* C 17- N 18$	12.78	0.82	0.091
n1 N 16	$\sigma^* C 17- N 19$	4.35	0.76	0.051
n1 N 18	$\sigma^* N 1- C 14$	3.01	0.79	0.044
n1 N 18	$\sigma^* O 7- H 26$	9.53	0.76	0.076
n1 N 18	$\sigma^* C 13- C 14$	9.63	0.87	0.082
n1 N 18	$\sigma^* N 16- C 17$	11.82	0.82	0.088
n1 N 19	$\pi^* C 17- N 18$	51.13	0.27	0.105
n1 O 20	$\sigma^* C 15- N 16$	7.44	1.03	0.078
n2 O 20	$\pi^* C 15- N 16$	51.24	0.31	0.113
n2 O 20	$\sigma^* C 21- H 35$	5.05	0.76	0.055
n2 O 20	$\sigma^* C 21- H 36$	5.14	0.76	0.056
$\sigma N 1- C 4$	$\sigma^* N 1- C 14$	1.02	1.14	0.031
$\sigma N 1- C 4$	$\sigma^* C 11- N 12$	0.89	1.26	0.03
$\sigma N 1- C 4$	$\sigma^* C 13- C 14$	0.93	1.22	0.03
$\sigma N 1- C 11$	$\sigma^* N 1- C 4$	1.03	1.01	0.029
$\sigma N 1- C 11$	$\sigma^* N 1- C 14$	1.36	1.16	0.036
$\sigma N 1- C 11$	$\sigma^* C 4- O 5$	0.91	1	0.027
$\sigma N 1- C 11$	$\sigma^* C 14- N 18$	5.27	1.21	0.071
$\sigma N 1- C 14$	$\sigma^* N 1- C 4$	1.09	1.04	0.03
$\sigma N 1- C 14$	$\sigma^* N 1- C 11$	1.23	1.14	0.033
$\sigma N 1- C 14$	$\sigma^* C 4- O 5$	0.94	1.02	0.028
$\sigma N 1- C 14$	$\sigma^* C 11- H 31$	1.82	1.21	0.042
$\sigma N 1- C 14$	$\sigma^* C 13- C 14$	0.73	1.26	0.027
$\sigma N 1- C 14$	$\sigma^* C 13- C 15$	2.12	1.26	0.046
$\sigma N 1- C 14$	$\sigma^* C 14- N 18$	0.93	1.24	0.03
$\sigma N 1- C 14$	$\sigma^* C 17- N 18$	1.44	1.23	0.037
$\sigma C 2- O 8$	$\sigma^* C 3- O 7$	1.4	1.05	0.034
$\sigma C 2- O 8$	$\sigma^* C 6- C 9$	1.17	1.11	0.032
$\sigma C 3- C 4$	$\sigma^* N 1- C 11$	2.01	0.97	0.039
$\sigma C 3- O 7$	$\sigma^* C 2- O 8$	1.21	1.02	0.031
$\sigma C 4- O 5$	$\sigma^* N 1- C 14$	1.73	1.21	0.041
$\sigma O 5- C 6$	$\sigma^* C 2- H 22$	1.15	1.16	0.033
$\sigma O 5- C 6$	$\sigma^* C 4- H 24$	0.95	1.17	0.03
$\sigma O 5- C 6$	$\sigma^* C 9- H 28$	0.93	1.14	0.029
$\sigma C 6- C 9$	$\sigma^* C 2- O 8$	2.32	0.84	0.039
$\sigma C 6- C 9$	$\sigma^* O 10- H 30$	1.45	0.98	0.034
$\sigma O 7- H 26$	$\sigma^* C 2- C 3$	3.11	1.02	0.05
$\sigma O 8- H 27$	$\sigma^* C 2- C 3$	2.85	1.03	0.048
$\sigma C 9- O 10$	$\sigma^* C 2- C 6$	1.6	1.08	0.037
$\sigma C 9- H 28$	$\sigma^* O 5- C 6$	5	0.77	0.055
$\sigma O 10- H 30$	$\sigma^* C 6- C 9$	2.8	1.04	0.048

Donor(i)	Acceptor(j)	E <sup>(2)a</sup> (kcal/mol)	E(j)-E(i) <sup>b</sup> (a.u.)	F(i,j) <sup>c</sup> (a.u.)
σ C 11- N 12	σ* N 1- C 4	2.04	1.03	0.041
σ C 11- N 12	σ* C 13- C 15	5.76	1.25	0.076
π C 11- N 12	π* C 13- C 14	20.55	0.32	0.073
σ N 12- C 13	σ* N 1- C 11	1.66	1.08	0.038
σ N 12- C 13	σ* C 11- H 31	4.5	1.15	0.064
σ N 12- C 13	σ* C 13- C 15	1.77	1.2	0.041
σ N 12- C 13	σ* C 14- N 18	2.92	1.17	0.052
σ C 13- C 14	σ* N 1- C 4	4.61	0.92	0.058
σ C 13- C 14	σ* C 15- O 20	4.35	1	0.059
π C 13- C 14	π* C 11- N 12	16.03	0.28	0.06
π C 13- C 14	π* C 15- N 16	36.69	0.26	0.087
π C 13- C 14	π* C 17- N 18	9.92	0.25	0.044
σ C 13- C 15	σ* N 1- C 14	2.12	1.09	0.043
σ C 13- C 15	σ* N 12- C 13	1.73	1.1	0.039
σ C 13- C 15	σ* O 20- C 21	2.79	0.89	0.045
σ C 14- N 18	σ* N 1- C 11	1.17	1.15	0.033
σ C 14- N 18	σ* C 13- C 14	1.92	1.27	0.044
σ C 14- N 18	σ* C 17- N 19	4.12	1.18	0.062
σ C 15- N 16	σ* N 12- C 13	2.52	1.21	0.049
σ C 15- N 16	σ* C 13- C 15	1.7	1.28	0.042
σ C 15- N 16	σ* C 17- N 19	3	1.19	0.053
π C 15- N 16	π* C 13- C 14	7.53	0.33	0.045
π C 15- N 16	π* C 17- N 18	40.96	0.3	0.099
σ C 15- O 20	σ* N 16- C 17	1.69	1.33	0.042
σ N 16- C 17	σ* C 15- O 20	4.12	1.12	0.061
σ N 16- C 17	σ* N 19- H 32	1.55	1.18	0.038
σ C 17- N 18	σ* N 1- C 14	6.47	1.19	0.078
σ C 17- N 18	σ* N 19- H 33	1.49	1.18	0.038
π C 17- N 18	σ* O 7- H 26	2.52	0.75	0.039
π C 17- N 18	π* C 13- C 14	32.64	0.33	0.093
π C 17- N 18	π* C 15- N 16	6.15	0.31	0.039
σ C 17- N 19	σ* C 14- N 18	2.05	1.25	0.045
σ C 17- N 19	σ* C 15- N 16	2.02	1.27	0.045
σ N 19- H 32	σ* N 16- C 17	4.03	1.12	0.06
σ N 19- H 32	π* C 17- N 18	0.79	0.61	0.02
σ N 19- H 33	σ* C 17- N 18	4.23	1.13	0.062
σ N 19- H 33	π* C 17- N 18	0.65	0.61	0.018
σ O 20- C 21	σ* C 13- C 15	3.16	1.27	0.057
σ O 7- H 26	π* C 17- N 18	0.57	0.66	0.017

<sup>a</sup>E<sup>(2)</sup> Energy of conjugative interactions; <sup>b</sup>Energy difference between donor and acceptor i and j NBOs; <sup>c</sup>F(i, j) is the Fock matrix element between i and j NBOs

**Table S3.** Predicted pharmacological activities of Nelarabine (3).

Pa	Pi	Pharmacological activities
0,973	0,002	Nucleotide metabolism regulator
0,959	0,002	Methylenetetrahydrofolate reductase (NADPH) inhibitor
0,936	0,002	ADP-thymidine kinase inhibitor
0,933	0,002	Nucleoside oxidase (H2O2-forming) inhibitor
0,921	0,002	Mitochondrial processing peptidase inhibitor
0,919	0,002	Antiviral (Poxvirus)
0,917	0,003	Cytostatic
0,913	0,003	NAD(P)+-arginine ADP-ribosyltransferase inhibitor
0,906	0,001	DNA repair enzyme inhibitor
0,908	0,008	CDP-glycerol glycerophosphotransferase inhibitor
0,892	0,005	Sphinganine kinase inhibitor
0,884	0,003	DNA synthesis inhibitor
0,883	0,005	Glucose oxidase inhibitor
0,883	0,006	TP53 expression enhancer
0,877	0,002	DNA directed DNA polymerase inhibitor
0,876	0,000	Urate-ribonucleotide phosphorylase inhibitor
0,874	0,002	Antiviral (Herpes)
0,873	0,008	Benzoate-CoA ligase inhibitor
0,864	0,007	Mannotetraose 2-α-N-acetylglucosaminyltransferase inhibitor
0,859	0,009	Glutamate-5-semialdehyde dehydrogenase inhibitor
0,849	0,002	Lipotropic
0,840	0,003	D-threo-aldehyde 1-dehydrogenase inhibitor

Pa	Pi	Pharmacological activities
0,831	0,002	Glutathione peroxidase inhibitor
0,829	0,003	Antineoplastic antimetabolite
0,825	0,003	Adenosine regulator
0,819	0,003	Antiviral (Picornavirus)
0,796	0,001	3'-Nucleotidase inhibitor
0,778	0,001	Glutathione synthase inhibitor
0,779	0,003	Alpha-1,6-mannosyl-glycoprotein 4-beta-N-acetylglucosaminyltransferase inhibitor
0,778	0,004	Antiprotozoal (Trypanosoma)
0,778	0,008	Lysine 2,3-aminomutase inhibitor
0,765	0,004	Undecaprenyl-phosphate mannosyltransferase inhibitor
0,760	0,002	Deoxyribonuclease X inhibitor
0,763	0,009	N-acetylneuraminate 7-O(or 9-O)-acetyltransferase inhibitor
0,763	0,011	Immunostimulant
0,752	0,007	Trans-acenaphthene-1,2-diol dehydrogenase inhibitor
0,752	0,011	Immunosuppressant
0,745	0,004	Cytochrome-b5 reductase inhibitor
0,740	0,001	Methylenetetrahydrofolate dehydrogenase (NADP+) inhibitor
0,742	0,005	Phosphatidate phosphatase inhibitor
0,748	0,011	2-Dehydropantoate 2-reductase inhibitor
0,741	0,005	Alcohol dehydrogenase (acceptor) inhibitor
0,737	0,003	Dynein ATPase inhibitor
0,737	0,002	Adenosine receptor antagonist
0,736	0,003	Nitrate reductase inhibitor
0,734	0,003	Adenylyl-sulfate reductase inhibitor
0,734	0,006	Histidine N-acetyltransferase inhibitor
0,729	0,004	Malate dehydrogenase (acceptor) inhibitor
0,725	0,002	Inositol oxygenase inhibitor
0,722	0,004	Ferredoxin-NADP+ reductase inhibitor
0,719	0,003	Glucose 1-dehydrogenase inhibitor
0,720	0,007	Vasodilator, coronary
0,714	0,002	Formate-dihydrofolate ligase inhibitor
0,710	0,002	FMN reductase inhibitor
0,711	0,005	Cyclohexanone monooxygenase inhibitor
0,705	0,003	GDP-mannose 6-dehydrogenase inhibitor
0,706	0,004	Na+-transporting two-sector ATPase inhibitor
0,703	0,002	ATP phosphoribosyltransferase inhibitor
0,705	0,004	Rubredoxin-NAD+ reductase inhibitor
0,703	0,003	Glutamine synthetase inhibitor
0,703	0,003	4-Nitrophenylphosphatase inhibitor
0,703	0,004	Malate dehydrogenase inhibitor
0,700	0,002	Adenine deaminase inhibitor
0,702	0,004	Antineoplastic (non-Hodgkin's lymphoma)
0,699	0,007	DNA-(apurinic or apyrimidinic site) lyase inhibitor
0,697	0,006	4-Hydroxyphenylacetate 3-monooxygenase inhibitor
0,694	0,006	H+-transporting two-sector ATPase inhibitor
0,687	0,005	Apyrase inhibitor
0,688	0,007	Cyclic AMP phosphodiesterase inhibitor
0,682	0,003	Chaperonin ATPase inhibitor
0,681	0,003	Malate oxidase inhibitor
0,678	0,001	Purine nucleosidase inhibitor
0,678	0,001	Mannitol-1-phosphate 5-dehydrogenase inhibitor
0,678	0,002	NADH dehydrogenase inhibitor
0,697	0,024	Lysase inhibitor
0,677	0,004	Pyruvate dehydrogenase inhibitor
0,674	0,003	Nucleoside-diphosphatase inhibitor
0,682	0,011	Vasodilator, peripheral
0,668	0,002	Adenosine A2 receptor antagonist
0,669	0,004	Cardioprotectant
0,669	0,005	Aspergillus nuclease S1 inhibitor
0,662	0,002	Phosphoglycerate dehydrogenase inhibitor
0,662	0,004	Thiamine-triphosphatase inhibitor
0,660	0,002	Galactokinase inhibitor
0,659	0,002	2-Oxaldehyde dehydrogenase (NAD+) inhibitor
0,662	0,010	Anticarcinogenic
0,657	0,005	Venom exonuclease inhibitor
0,670	0,023	HIF1A expression inhibitor



Pa	Pi	Pharmacological activities
0,650	0,002	Acyloxyacyl hydrolase inhibitor
0,671	0,031	Antineoplastic
0,658	0,019	Prostaglandin-E2 9-reductase inhibitor
0,640	0,003	Glycogen (starch) synthase inhibitor
0,640	0,003	RELA expression inhibitor
0,639	0,003	Adenosine A1 receptor antagonist
0,639	0,003	Formaldehyde dehydrogenase (glutathione) inhibitor
0,639	0,003	Antimetabolite
0,636	0,002	Adenosylmethionine-8-amino-7-oxononanoate transaminase inhibitor
0,636	0,002	Adenosine deaminase inhibitor
0,635	0,001	Ribose-5-phosphate-ammonia ligase inhibitor
0,644	0,010	Antiviral (Influenza)
0,634	0,001	Ketohexokinase inhibitor
0,637	0,005	3'-Demethylstaurosporine O-methyltransferase inhibitor
0,639	0,009	Chitinase inhibitor
0,634	0,005	4-Coumarate-CoA ligase inhibitor
0,632	0,004	Acyl-CoA hydrolase inhibitor
0,632	0,004	Palmitoyl-CoA hydrolase inhibitor
0,633	0,006	Sulfite dehydrogenase inhibitor
0,629	0,004	Laminaribiose phosphorylase inhibitor
0,625	0,001	Biotin carboxylase inhibitor
0,624	0,002	Adenosine A2a receptor antagonist
0,623	0,001	Hypoxanthine phosphoribosyltransferase inhibitor
0,618	0,003	N6-methyl-lysine oxidase inhibitor
0,624	0,010	Radiosensitizer
0,617	0,004	Ethanolaminephosphotransferase inhibitor
0,615	0,005	Channel-conductance-controlling ATPase inhibitor
0,614	0,005	Pancreatic ribonuclease inhibitor
0,611	0,003	Ethanolamine kinase inhibitor
0,611	0,005	Choline kinase inhibitor
0,605	0,001	Aspartate carbamoyltransferase inhibitor
0,605	0,002	Sulfate adenylyltransferase inhibitor
0,607	0,004	Sedoheptulose-bisphosphatase inhibitor
0,606	0,003	Pyruvate carboxylase inhibitor
0,606	0,003	N-acetylneuraminase 4-O-acetyltransferase inhibitor
0,605	0,003	Serratia marcescens nuclease inhibitor
0,602	0,002	Cysteine-tRNA ligase inhibitor
0,600	0,002	Lactoylglutathione lyase inhibitor
0,598	0,002	Adenylyl-sulfate kinase inhibitor
0,600	0,004	Glutamate dehydrogenase [NAD(P)+] inhibitor
0,610	0,019	Ecdysone 20-monooxygenase inhibitor
0,595	0,004	Acetate-CoA ligase inhibitor
0,592	0,005	Sulfur dioxygenase inhibitor
0,587	0,002	Adenylylsulphatase inhibitor
0,589	0,003	Phosphofructokinase-1 inhibitor
0,589	0,004	Dethiobiotin synthase inhibitor
0,588	0,004	Polyribonucleotide nucleotidyltransferase inhibitor
0,581	0,002	Dolichol kinase inhibitor
0,582	0,002	ATP adenylyltransferase inhibitor
0,584	0,004	Arylamine N-acetyltransferase inhibitor
0,582	0,005	Heat shock protein 27 antagonist
0,582	0,005	Thiopurine S-methyltransferase inhibitor
0,587	0,011	Mycothiol-S-conjugate amidase inhibitor
0,576	0,002	Hydroxyacylglutathione hydrolase inhibitor
0,581	0,006	Glycerol dehydrogenase inhibitor
0,578	0,004	Diacylglycerol cholinephosphotransferase inhibitor
0,577	0,003	Glutaminy-peptide cyclotransferase inhibitor
0,576	0,004	Phosphatidate cytidylyltransferase inhibitor
0,574	0,003	Aryl-aldehyde dehydrogenase (NADP+) inhibitor
0,574	0,003	Sulfate adenylyltransferase (ADP) inhibitor
0,592	0,022	Biotinidase inhibitor
0,571	0,002	Sterol 3-beta-glucosyltransferase inhibitor
0,569	0,000	Galactoside 2-alpha-L-fucosyltransferase inhibitor
0,570	0,002	N-formylglutamate deformylase inhibitor
0,574	0,006	CDK9/cyclin T1 inhibitor
0,571	0,003	Thiamine-phosphate kinase inhibitor

Pa	Pi	Pharmacological activities
0,573	0,005	Metabolic disease treatment
0,572	0,005	Formate dehydrogenase inhibitor
0,569	0,002	3-Hydroxyanthranilate oxidase inhibitor
0,576	0,011	Bilirubin oxidase inhibitor
0,568	0,005	RNA directed DNA polymerase inhibitor
0,564	0,003	Glycerol-3-phosphate dehydrogenase (NAD+) inhibitor
0,572	0,013	Proliferative diseases treatment
0,560	0,000	Ribosylpyrimidine nucleosidase inhibitor
0,565	0,008	4-Hydroxybenzoate nonaprenyltransferase inhibitor
0,558	0,002	Xanthommatin reductase inhibitor
0,560	0,003	Procollagen glucosyltransferase inhibitor
0,562	0,006	L-threonine 3-dehydrogenase inhibitor
0,560	0,005	Acylglycerone-phosphate reductase inhibitor
0,554	0,001	Cytosine deaminase inhibitor
0,557	0,004	Choline sulfotransferase inhibitor
0,566	0,013	Isopenicillin-N epimerase inhibitor
0,554	0,001	Adenine phosphoribosyltransferase inhibitor
0,552	0,006	Guanidinoacetate N-methyltransferase inhibitor
0,547	0,002	NAD(P)+ transhydrogenase (B-specific) inhibitor
0,548	0,004	N-(5-amino-5-carboxypentanoyl)-L-cysteinyl-D-valine synthase inhibitor
0,545	0,002	Sepiapterin reductase inhibitor
0,545	0,003	Antiviral (Hepatitis B)
0,544	0,002	Pyrroline-5-carboxylate reductase inhibitor
0,543	0,003	Fumarate hydratase inhibitor
0,547	0,009	Alpha-Methylacyl-CoA racemase inhibitor
0,543	0,005	DNA polymerase I inhibitor
0,538	0,002	Xanthine phosphoribosyltransferase inhibitor
0,539	0,004	Saccharopine dehydrogenase (NAD+, L-lysine-forming) inhibitor
0,536	0,002	DNA nucleotidylexotransferase inhibitor
0,535	0,003	Isovaleryl-CoA dehydrogenase inhibitor
0,550	0,018	NADPH-ferrihemoprotein reductase inhibitor
0,537	0,006	Glycine-tRNA ligase inhibitor
0,534	0,005	tRNA adenylyltransferase inhibitor
0,567	0,039	UDP-N-acetylglucosamine 4-epimerase inhibitor
0,537	0,010	Glyoxylate reductase (NADP+) inhibitor
0,527	0,001	Uridine nucleosidase inhibitor
0,530	0,006	Myosin-light-chain-phosphatase inhibitor
0,525	0,001	Pyruvate, phosphate dikinase inhibitor
0,526	0,003	Polynucleotide 5'-hydroxy-kinase inhibitor
0,527	0,004	Adenylate cyclase inhibitor
0,542	0,020	Lactase inhibitor
0,534	0,012	Antileukemic
0,525	0,005	DNA ligase (ATP) inhibitor
0,521	0,003	Beta-fructofuranosidase inhibitor
0,523	0,006	RNA synthesis inhibitor
0,523	0,006	Antiviral
0,519	0,003	Glycine N-methyltransferase inhibitor
0,520	0,003	Inosine nucleosidase inhibitor
0,518	0,002	ADP-ribosylarginine hydrolase inhibitor
0,516	0,001	Adenylosuccinate synthase inhibitor
0,517	0,003	5-Formyltetrahydrofolate cyclo-ligase inhibitor
0,516	0,003	Nicotinate-nucleotide diphosphorylase (carboxylating) inhibitor
0,524	0,011	CDP-diacylglycerol-serine O-phosphatidyltransferase inhibitor
0,515	0,003	Adenylate cyclase V inhibitor
0,516	0,004	Aminoacyl-tRNA synthetase inhibitor
0,515	0,003	Carbamoyl-phosphate synthase (ammonia) inhibitor
0,513	0,002	Orotate phosphoribosyltransferase inhibitor
0,528	0,017	Transcription factor stimulant
0,528	0,017	Transcription factor NF kappa B stimulant
0,512	0,003	NAD+ kinase inhibitor
0,519	0,013	DELTA14-sterol reductase inhibitor
0,515	0,009	4-Chlorobenzoyl-CoA dehalogenase inhibitor
0,510	0,004	(N-acetylneuraminy)-galactosylglucosylceramide N-acetylgalactosaminyltransferase inhibitor
0,507	0,002	Sucrose synthase inhibitor
0,517	0,011	Antineoplastic (solid tumors)
0,507	0,004	Glutamate dehydrogenase inhibitor

Pa	Pi	Pharmacological activities
0,507	0,005	tRNA cytidyltransferase inhibitor
0,506	0,004	Glucosyl transferase inhibitor
0,501	0,001	Poly(ADP-ribose) glycohydrolase inhibitor
0,500	0,002	NAD <sup>+</sup> nucleosidase inhibitor
0,520	0,024	Cyclic AMP agonist
0,497	0,001	GMP synthase inhibitor
0,497	0,004	Adenosine A3 receptor antagonist
0,496	0,003	tRNA (guanine-N1-)-methyltransferase inhibitor
0,496	0,004	CMP-N-acetylneuraminate monooxygenase inhibitor
0,504	0,013	Diamine N-acetyltransferase inhibitor
0,491	0,004	5-Aminolevulinate synthase inhibitor
0,489	0,002	Methionine adenosyltransferase inhibitor
0,490	0,004	Heparan-alpha-glucosaminide N-acetyltransferase inhibitor
0,500	0,016	Nitrite reductase [NAD(P)H] inhibitor
0,497	0,013	Succinate-semialdehyde dehydrogenase [NAD(P) <sup>+</sup> ] inhibitor
0,491	0,007	Endopeptidase La inhibitor
0,484	0,000	Glycoprotein 3-alpha-L-fucosyltransferase inhibitor
0,527	0,044	G-protein-coupled receptor kinase inhibitor
0,527	0,044	Beta-adrenergic receptor kinase inhibitor
0,482	0,002	Glucose-1-phosphate adenylyltransferase inhibitor
0,481	0,002	Nicotinate phosphoribosyltransferase inhibitor
0,491	0,012	Guanidinoacetate kinase inhibitor
0,489	0,010	Glutamate-tRNA ligase inhibitor
0,496	0,020	Antimetastatic
0,482	0,006	[acyl-carrier-protein] S-acetyltransferase inhibitor
0,489	0,014	Aldehyde dehydrogenase (NADP <sup>+</sup> ) inhibitor
0,478	0,003	Polar-amino-acid-transporting ATPase inhibitor
0,478	0,005	Cyclopropane-fatty-acyl-phospholipid synthase inhibitor
0,474	0,003	Chitin synthase inhibitor
0,477	0,008	Dolichyl-phosphate beta-glucosyltransferase inhibitor
0,473	0,008	Alkylator
0,467	0,005	UDP-glucose-hexose-1-phosphate uridylyltransferase inhibitor
0,463	0,003	Tryptophan-tRNA ligase inhibitor
0,461	0,001	Guanylate kinase inhibitor
0,464	0,004	NAD(P) <sup>+</sup> transhydrogenase (AB-specific) inhibitor
0,459	0,002	tRNA methyltransferase inhibitor
0,458	0,001	ATP diphosphatase inhibitor
0,462	0,005	Inositol-polyphosphate 5-phosphatase inhibitor
0,458	0,002	Geranylgeranyl-diphosphate geranylgeranyltransferase inhibitor
0,473	0,018	Prenyl-diphosphatase inhibitor
0,454	0,004	Antiprotozoal (Trichomonas)
0,451	0,003	Nicotinamide-nucleotide adenylyltransferase inhibitor
0,486	0,037	Alcohol O-acetyltransferase inhibitor
0,447	0,001	Ribose-5-phosphate isomerase inhibitor
0,448	0,004	Protein-synthesizing GTPase inhibitor
0,447	0,003	Alpha, alpha-trehalose phosphorylase (configuration-retaining) inhibitor
0,444	0,001	Thiamine-phosphate diphosphorylase inhibitor
0,442	0,002	Gluconokinase inhibitor
0,468	0,029	D-lactaldehyde dehydrogenase inhibitor
0,442	0,004	Vasculitis treatment
0,441	0,004	UDP-glucuronate decarboxylase inhibitor
0,440	0,004	Malate-CoA ligase inhibitor
0,439	0,004	Adenylate kinase inhibitor
0,442	0,008	DNA directed RNA polymerase inhibitor
0,436	0,002	Phenylalanine-tRNA ligase inhibitor
0,456	0,027	Vasodilator
0,438	0,008	Pyruvate dehydrogenase (lipoamide) inhibitor
0,436	0,007	Aldehyde dehydrogenase (NAD <sup>+</sup> ) inhibitor
0,433	0,004	Pyruvate kinase inhibitor
0,433	0,005	Uric acid excretion stimulant
0,430	0,003	FAD diphosphatase inhibitor
0,456	0,031	Antiprotozoal (Leishmania)
0,451	0,027	P-benzoquinone reductase (NADPH) inhibitor
0,430	0,006	Glutathione-disulfide reductase inhibitor
0,424	0,002	Ribonuclease U2 inhibitor
0,436	0,014	N-acetyllactosamine synthase inhibitor

Pa	Pi	Pharmacological activities
0,426	0,004	Alpha, alpha-trehalase inhibitor
0,451	0,029	Phosphopantothenoylcysteine decarboxylase inhibitor
0,423	0,003	Bis(5'-adenosyl)-triphosphatase inhibitor
0,422	0,002	Beta-galactoside alpha-2,3-sialyltransferase inhibitor
0,419	0,001	S-methyl-5-thioadenosine phosphorylase inhibitor
0,420	0,002	Chondroitin 6-sulfotransferase inhibitor
0,420	0,003	Phosphoenolpyruvate carboxykinase (GTP) inhibitor
0,418	0,002	Phosphogluconate dehydrogenase (decarboxylating) inhibitor
0,424	0,009	Antineoplastic (lymphoma)
0,420	0,004	[phosphorylase] phosphatase inhibitor
0,419	0,004	Octadecanal decarbonylase inhibitor
0,417	0,002	CDP-diacylglycerol-inositol 3-phosphatidyltransferase inhibitor
0,419	0,005	NAD <sup>+</sup> -dinitrogen-reductase ADP-D-ribosyltransferase inhibitor
0,460	0,046	Aspartyltransferase inhibitor
0,423	0,010	Aryl sulfotransferase inhibitor
0,437	0,025	Undecaprenyldiphospho-muramoylpentapeptide beta-N-acetylglucosaminyltransferase inhibitor
0,422	0,011	Phospholipase A1 inhibitor
0,412	0,001	UDP-N-acetylglucosamine-dolichyl-phosphate N-acetylglucosaminophosphotransferase inhibitor
0,411	0,004	Argininosuccinate synthase inhibitor
0,416	0,009	Glutamate 5-kinase inhibitor
0,437	0,032	Glycerol-3-phosphate oxidase inhibitor
0,407	0,001	AMP nucleosidase inhibitor
0,407	0,004	Glucosamine 6-phosphate N-acetyltransferase inhibitor
0,406	0,004	D-malate dehydrogenase (decarboxylating) inhibitor
0,404	0,002	Galactosylceramide sulfotransferase inhibitor
0,415	0,016	Dihydrodipicolinate reductase inhibitor
0,410	0,012	Lactose synthase inhibitor
0,433	0,038	N-hydroxyarylamine O-acetyltransferase inhibitor
0,396	0,001	Glycoprotein-fucosylgalactoside alpha-N-acetylglactosaminyltransferase inhibitor
0,399	0,004	Sucrose-phosphate synthase inhibitor
0,399	0,005	Acyl-CoA oxidase inhibitor
0,396	0,003	Acetyl-CoA C-acyltransferase inhibitor
0,394	0,003	ATP citrate synthase inhibitor
0,391	0,001	Ribose-phosphate diphosphokinase inhibitor
0,391	0,002	Dolichyl-phosphate beta-D-mannosyltransferase inhibitor
0,392	0,003	GlutaminytRNA synthase (glutamine-hydrolysing) inhibitor
0,393	0,005	Glyceraldehyde-3-phosphate dehydrogenase (phosphorylating) inhibitor
0,390	0,003	Pyruvate, water dikinase inhibitor
0,405	0,019	Myosin ATPase inhibitor
0,388	0,003	Guanine deaminase inhibitor
0,388	0,004	Fructose-2,6-bisphosphate 2-phosphatase inhibitor
0,386	0,003	CMP-N-acylneuraminate phosphodiesterase inhibitor
0,407	0,024	MAP3K5 inhibitor
0,408	0,026	Immunomodulator
0,391	0,009	D-Octopine dehydrogenase inhibitor
0,384	0,004	Phosphate acetyltransferase inhibitor
0,384	0,004	Guanylate cyclase inhibitor
0,381	0,001	GTP cyclohydrolase I inhibitor
0,394	0,015	N-acetylglucosaminide beta-1,3-N-acetylglucosaminyltransferase inhibitor
0,381	0,004	Pteridine reductase inhibitor
0,379	0,003	Citrate (Si)-synthase inhibitor
0,399	0,023	Levansucrase inhibitor
0,390	0,016	Acetate kinase inhibitor
0,376	0,002	Thymidine kinase 1 inhibitor
0,376	0,002	Nucleotide diphosphatase inhibitor
0,381	0,007	UDP-glucose 4-epimerase inhibitor
0,379	0,005	Purine biosynthesis inhibitor
0,375	0,001	NMN nucleosidase inhibitor
0,379	0,006	Magnesium-protoporphyrin IX methyltransferase inhibitor
0,389	0,017	Inorganic diphosphatase inhibitor
0,376	0,004	N-acetylglucosamine kinase inhibitor
0,371	0,002	Thymidine kinase inhibitor
0,374	0,006	Glutamate synthase (NADPH) inhibitor
0,400	0,033	Macrophage stimulant
0,371	0,005	Gout treatment
0,395	0,028	Ethanolamine-phosphate cytidyltransferase inhibitor

Pa	Pi	Pharmacological activities
0,368	0,001	Fructokinase inhibitor
0,365	0,001	Ribonuclease inhibitor
0,411	0,048	MMP9 expression inhibitor
0,410	0,047	Chemosensitizer
0,364	0,002	Phosphoglucomutase inhibitor
0,364	0,002	Nucleoside deoxyribosyltransferase inhibitor
0,408	0,047	RNA-directed RNA polymerase inhibitor
0,365	0,004	Site-specific DNA-methyltransferase (adenine-specific) inhibitor
0,360	0,002	Methylthioadenosine nucleosidase inhibitor
0,360	0,002	DNA methylase inhibitor
0,357	0,002	Diacylglycerol kinase inhibitor
0,358	0,004	Phosphoribulokinase inhibitor
0,355	0,002	[hydroxymethylglutaryl-CoA reductase (NADPH)] kinase inhibitor
0,361	0,008	Cholate-CoA ligase inhibitor
0,358	0,006	Protein-S-isoprenylcysteine O-methyltransferase inhibitor
0,357	0,005	Cytidine deaminase inhibitor
0,364	0,013	Respiratory distress syndrome treatment
0,354	0,003	Rhodopsin kinase inhibitor
0,353	0,003	6-Phosphofructo-2-kinase inhibitor
0,356	0,006	Valine-tRNA ligase inhibitor
0,405	0,055	Membrane permeability enhancer
0,355	0,005	Hydroxymethylglutaryl-CoA lyase inhibitor
0,350	0,001	Arginine-tRNA ligase inhibitor
0,354	0,005	Malate synthase inhibitor
0,353	0,004	Asparagine synthase (glutamine-hydrolysing) inhibitor
0,369	0,025	Antiprotozoal
0,350	0,007	Estrone sulfotransferase inhibitor
0,344	0,002	5'-Nucleotidase inhibitor
0,354	0,012	Apoptosis antagonist
0,445	0,104	Sugar-phosphatase inhibitor
0,342	0,002	Purine antagonist
0,360	0,021	Sweetener
0,348	0,009	Acetolactate decarboxylase inhibitor
0,349	0,011	Butyrate-CoA ligase inhibitor
0,357	0,019	Mannosyl-glycoprotein endo-beta-N-acetylglucosaminidase inhibitor
0,346	0,012	Succinate-CoA ligase (ADP-forming) inhibitor
0,339	0,005	Thiol S-methyltransferase inhibitor
0,338	0,004	CTP synthase inhibitor
0,351	0,018	Antiviral (Influenza A)
0,336	0,004	Nicotinamide phosphoribosyltransferase inhibitor
0,334	0,002	Polynucleotide adenyltransferase inhibitor
0,343	0,011	Benzoylformate decarboxylase inhibitor
0,337	0,006	Malate dehydrogenase (oxaloacetate-decarboxylating) inhibitor
0,333	0,003	Xanthine dehydrogenase inhibitor
0,345	0,015	Analgesic stimulant
0,341	0,013	Glycerone-phosphate O-acyltransferase inhibitor
0,328	0,001	Polyphosphate kinase inhibitor
0,330	0,003	rRNA (adenosine-2'-O-)-methyltransferase inhibitor
0,331	0,007	D-lactate dehydrogenase inhibitor
0,327	0,003	Nucleoside transporters inhibitor
0,328	0,004	Neolactotetraosylceramide alpha-2,3-sialyltransferase inhibitor
0,326	0,002	2-Methylcitrate synthase inhibitor
0,326	0,003	Formate C-acetyltransferase inhibitor
0,329	0,006	Ornithine carbamoyltransferase inhibitor
0,325	0,003	[acetyl-CoA carboxylase] kinase inhibitor
0,373	0,053	1-Alkylglycerophosphocholine O-acetyltransferase inhibitor
0,321	0,002	UDP-N-acetylglucosamine-lysosomal-enzyme N-acetylglucosaminophosphotransferase inhibitor
0,323	0,005	dUTP diphosphatase inhibitor
0,335	0,019	Ceramide glucosyltransferase inhibitor
0,318	0,004	S-methyl-5-thioribose kinase inhibitor
0,316	0,002	Globoside alpha-N-acetylgalactosaminyltransferase inhibitor
0,337	0,023	2-Acylglycerol O-acyltransferase inhibitor
0,318	0,004	Biliverdin reductase inhibitor
0,316	0,003	Hydroxypyruvate reductase inhibitor
0,322	0,009	Aromatic-hydroxylamine O-acetyltransferase inhibitor
0,319	0,008	Purinergic P2X3 antagonist

Pa	Pi	Pharmacological activities
0,354	0,044	Pyroglutamyl-peptidase II inhibitor
0,322	0,013	Acetoin dehydrogenase inhibitor
0,310	0,001	UDP-sugar diphosphatase inhibitor
0,312	0,004	tRNA (cytosine-5-)-methyltransferase inhibitor
0,309	0,001	Methenyltetrahydrofolate cyclohydrolase inhibitor
0,324	0,018	Glucosamine-6-phosphate deaminase inhibitor
0,318	0,012	Serine-phosphoethanolamine synthase inhibitor
0,305	0,002	Procollagen galactosyltransferase inhibitor
0,316	0,015	Antineoplastic (lymphocytic leukemia)
0,383	0,084	Glucan endo-1,6-beta-glucosidase inhibitor
0,303	0,009	Dimethylhistidine N-methyltransferase inhibitor
0,302	0,009	Glycine N-acyltransferase inhibitor
0,302	0,011	Homocitrate synthase inhibitor
0,372	0,085	Beta glucuronidase inhibitor
0,323	0,041	Antitoxic
0,304	0,023	3-Methylbutanal reductase inhibitor
0,333	0,053	X-methyl-His dipeptidase inhibitor
0,337	0,062	Antiviral (Adenovirus)
0,377	0,103	Antianginal
0,356	0,091	Acetylgalactosaminyl-O-glycosyl-glycoprotein beta-1,3-N-acetylglucosaminyltransferase inhibitor
0,312	0,052	Fructan beta-fructosidase inhibitor
0,314	0,080	Dolichyl-diphosphooligosaccharide-protein glycotransferase inhibitor
0,311	0,080	Radioprotector
0,305	0,078	Antimycobacterial
0,331	0,104	Interleukin 2 agonist
0,320	0,099	Manganese peroxidase inhibitor
0,314	0,094	Exoribonuclease II inhibitor
0,341	0,141	Glucan endo-1,3-beta-D-glucosidase inhibitor
0,301	0,122	Polarisation stimulant
0,309	0,169	Erythropoiesis stimulant

Pa, probability to be active; Pi, probability to be inactive

**Table S4.** Main expected adverse reactions of Nelarabine (3).

Pa	Pi	Adverse reactions
0,954	0,004	Acidosis
0,925	0,002	Hyperuricemia
0,911	0,002	Splenomegaly
0,903	0,005	Sweating
0,903	0,010	Diarrhea
0,885	0,011	Stomatitis
0,845	0,002	Ototoxicity
0,848	0,010	Agranulocytosis
0,839	0,012	Thrombocytopenia
0,820	0,013	Leukopenia
0,796	0,015	Inflammation
0,789	0,017	Respiratory failure
0,787	0,016	Anemia
0,772	0,024	Headache
0,772	0,028	Nausea
0,766	0,027	Emetic
0,747	0,031	Pain
0,721	0,018	Coma
0,714	0,015	Bronchoconstrictor
0,730	0,039	Toxic, gastrointestinal
0,705	0,014	Cyanosis
0,709	0,019	Thrombophlebitis
0,705	0,037	Dermatitis
0,696	0,030	Hepatitis
0,693	0,033	Hyperglycemic
0,679	0,020	Psychoses
0,696	0,041	Fibrillation, atrial
0,688	0,033	Excitability
0,674	0,020	Optic neuritis
0,682	0,032	Nephrotoxic
0,683	0,042	Sensory disturbance
0,652	0,019	Allergic dermatitis



<b>Pa</b>	<b>Pi</b>	<b>Adverse reactions</b>
0,659	0,029	Weight loss
0,664	0,045	Dizziness
0,665	0,049	Hematotoxic
0,624	0,015	Demyelination
0,640	0,033	Optic neuropathy
0,625	0,031	Paralysis
0,622	0,050	Tachycardiac
0,583	0,015	Cytotoxic
0,601	0,061	Toxic, respiration
0,585	0,054	Hypotension
0,583	0,058	Dysarthria
0,529	0,015	Fasciculation
0,524	0,022	Acidosis, lactic
0,526	0,027	Fatty liver
0,534	0,044	Teratogen
0,554	0,070	Toxic
0,520	0,045	Embryotoxic
0,543	0,070	Hypertensive
0,514	0,051	Keratopathy
0,496	0,037	Torsades de pointes
0,525	0,077	Consciousness alteration
0,502	0,065	Neurotoxic
0,517	0,094	Ulcer, aphthous
0,499	0,078	Hepatotoxic
0,485	0,076	Ataxia
0,494	0,112	Conjunctivitis
0,391	0,010	Carcinogenic, group 2A
0,457	0,078	Hyperthermic
0,469	0,101	Sleep disturbance
0,433	0,067	Cholestasis
0,447	0,107	Ocular toxicity
0,442	0,106	Necrosis
0,410	0,085	Photoallergy dermatitis
0,385	0,118	Tremor
0,390	0,145	Drowsiness
0,354	0,159	Respiratory impairment
0,325	0,134	Gastrointestinal disturbance
0,338	0,154	Behavioral disturbance
0,316	0,164	Myocarditis
0,345	0,197	Xerostomia
0,304	0,164	Allergic contact dermatitis
0,324	0,222	Bradycardic

Pa, probability to be active; Pi, probability to be inactive